AN ABSTRACT OF THE THESIS OF

Scott W. Indermuehle for the degree of Master of Science in Mechanical Engineering presented on April 14, 1998. Title: Thermal Characterization Technique for Thin Dielectric Films.

Abstract approved: Redacted for Privacy

Richard B. Peterson

A phase sensitive measurement technique that permits the simultaneous determination of two independent thermal properties of thin dielectric films is presented. Applying the technique results in a film's thermal diffusivity and effusivity, from which the thermal conductivity and specific heat can be calculated. The technique involves measuring a specimen's front surface temperature response to a periodic heating signal. The heating signal is produced by passing current through a thin layer of nichrome that is deposited on the specimen's surface, and the temperature response is measured with a HgCdTe infrared detector operating at 77 K. The signal that is produced by the infrared detector is first conditioned, and then sent to a lock-in amplifier. The lock-in is used to extract the phase shift present between the temperature and heating signal through a frequency range of 500 Hz - 20 kHz. The corresponding phase data is fit to an analytical model using thermal diffusivity and effusivity as fitting parameters. The method has been applied effectively to 1.72 μm films of SiO_2 that have been thermally grown on a silicon substrate. Thermal properties have been obtained through a temperature range of 25°C - 300°C. One unanticipated outcome stemming from analysis of the experimental data is the ability to extract both the thermal conductivity and specific heat of a thin film from phase information alone, with no need for signal magnitude. This improves the overall utility of the measurement process and provides a 'clean', direct path with fewer assumptions between data and final results. The thermal properties determined so far with this method are consistent with past work on SiO_2 films.

Thermal Characterization Technique for Thin Dielectric Films

by

Scott W. Indermuehle

A THESIS

submitted to

Oregon State University

in partial fulfillment of
the requirements for the
degree of

Master of Science

Presented April 14, 1998
Commencement June 1998

Master of Science thesis of Scott W. Indermuehle presented on April 14, 1998

APPROVED:

Redacted for Privacy

Major Professor, representing Mechanical Engineering

Redacted for Privacy

Chair of Department of Mechanical Engineering

Redacted for Privacy

Dean of Graduate School

I understand that my thesis will become part of the permanent collection of Oregon State University libraries. My signature below authorizes release of my thesis to any reader upon request.

Redacted for Privacy

Scott W. Indermuehle, Author

Acknowledgments

The author would like to express his appreciation to Professor Rich Peterson, whose guidance has been a major contributor to the success of this project. Thanks go to Professor Tom Plant for his help with the nichrome deposition process that was used to produce the heating strips. The author would like to recognize Manfred Dittrich and Steve Adams for their help in fabricating various components of the experimental apparatus. The support received from Jennifer Rogers, family, and friends is also greatly appreciated. Finally, a much-deserved thank you goes to Hewlett Packard for making the thermal characterization project possible.

TABLE OF CONTENTS

LIST OF FIGURES

LIST OF FIGURES (Continued)

LIST OF TABLES

LIST OF ABBREVIATIONS AND SYMBOLS

A, B	Constants of Integration in Single Domain Model
A_1, A_2, B_1, B_2	Constants of Integration in Two Domain Model
C_p	Specific Heat
C_{p1}	Specific Heat of Thin Film
C_{p2}	Specific Heat of Substrate
e	Exponential
e_1	Thermal Effusivity of Thin Film
e_2	Thermal Effusivity of Substrate
E	Variable used for Simplification
f	Frequency
g	Rate of Volumetric Energy Generation
g_o	Amplitude of Periodic Boundary Condition
i	Complex Number $\sqrt{-1}$
I	Electrical Current
IMAG	Complex Variable used for Simplification
k	Thermal Conductivity
k_1	Thermal Conductivity of Thin Film
k_2	Thermal Conductivity of Substrate
L	Thickness of Thin Film
MAG	Magnitude of Temperature Response at Surface
q"	Heat Flux

LIST OF ABBREVIATIONS AND SYMBOLS (Continued)

R	Electrical Resistance
REAL	Variable used for Simplification
RMS	Root Mean Square
RSS	Root Sum Square
S	Temperature (Shifted Boundary Condition)
S_1	Temperature in Domain 1 (Shifted Boundary Condition)
S_2	Temperature in Domain 2 (Shifted Boundary Condition)
T	Temperature
T_1	Temperature in Domain 1
T_2	Temperature in Domain 2
T_{brass}	Heat Sink Temperature
$T_{surface}$	Specimen Surface Temperature
t	Time Coordinate
W	Temperature (Complex Combination)
W_1	Temperature in Domain 1 (Complex Combination)
W_2	Temperature in Domain 2 (Complex Combination)
x	Spatial Coordinate in Rectilinear System
y	Spatial Coordinate in Rectilinear System
z	Spatial Coordinate in Rectilinear System

LIST OF ABBREVIATIONS AND SYMBOLS (Continued)

α	Thermal Diffusivity
α_1	Thermal Diffusivity of Thin Film
α_2	Thermal Diffusivity of Substrate
ρ	Mass Density
ρ_1	Mass Density of Thin Film
ρ_2	Mass Density of Substrate
θ	Time Coordinate
ϕ	Phase Shift
Γ	Variable used for Simplification
ψ	Complex Combination Solution Function
ψ_1	Complex Combination Solution Function (Domain 1)
ψ_2	Complex Combination Solution Function (Domain 2)
ξ_1	Complex Variable used for Simplification
ξ_2	Complex Variable used for Simplification
μ	Thermal Penetration Depth
ω	Angular Frequency

THERMAL CHARACTERIZATION TECHNIQUE FOR THIN DIELECTRIC FILMS

1. INTRODUCTION

Thermal property characterization of very thin films is often a necessary first step in understanding the response that a microstructure will have when exposed to a transient heat input. Many technologically important microstructures are fabricated with layers of thin films, where each layer has unique thermal characteristics. Without accurate knowledge of both the thermal conductivity and specific heat of the various layers, modeling the temperature response of the structure is of little value. For instance, modeling an electronic component's ability to dissipate heat might be of interest. Because an electronic component depends on the passage of electric current for operation, self-heating is unavoidable. The continued miniaturization of electronic systems has resulted in a dramatic increase in the amount of heat generated per unit system volume, which in some cases is comparable in magnitude to those encountered in nuclear reactors and the surface of the sun.[1] Unless a system is properly designed, such high rates of heat generation will result in device failure. Without accurate knowledge of thermal properties, designing for thermal control is a difficult task.

A number of experimental challenges exist when thermal characterization of a thin film is sought. For one, standard methods used for bulk samples will often fail when applied to thin films due to the small dimensions involved. The thickness of a typical film may be on the order of 10 μm - 50 μm. However, as long as industry continues to increase component density, the film sizes needed to accommodate this trend will continually decrease. At this point in time the use of films in the sub-micron range is not uncommon, where size dependent effects will likely dictate thermal behavior.[2] The thermal properties of a film may also be dependent on the process used for its fabrication,[3] further increasing variation with respect to bulk

values. This makes a thin film's thermal characterization even more critical if accurate structure modeling is desired.

The pages herein describe a new thermal characterization technique that allows for simultaneous determination of two independent thermal properties of thin dielectric films. An analytical model is developed in detail, and a description of the experimental testing method is given. The technique is applied to a 1.72 μm film of SiO_2 thermally grown onto a silicon substrate. The data from these trials is analyzed, and results are presented with a comparison against those of bulk material. The paper concludes with a few brief remarks on the overall measurement technique and offers an indication as to possible future studies.

2. BACKGROUND

In the discipline of heat transfer there are numerous properties used for quantifying thermal characteristics of a solid material. However, only a select few of these properties often show up in analysis. Therefore, the following discussion will be limited to the important properties of thermal conductivity (k), thermal diffusivity (α), and specific heat (C_p). A description of each property is provided in this chapter, along with a brief overview of experimental techniques that have been developed to obtain values for these properties in past work on thin film materials.

Conduction as defined by Incropera and Dewitt[4] is the transfer of energy from more energetic particles of a substance to neighboring particles of less energy as a result of interaction between the particles. A material in the solid state can be viewed as atoms bound in a periodic arrangement, and possibly of electrons that are free to move throughout the solid. Therefore, two vehicles are available for conduction of heat in a solid. First, thermal conduction can occur by migration of the free electrons through the solid structure. Because of their abundance in a pure metal, free electrons contribute heavily to this type of material's ability to conduct heat. Second, energy can be transferred by molecular vibration within a solid. Conduction in a non-metal occurs solely through this vehicle because free electrons are not available for migration. It should be noted that heat conduction through a material such as an alloy is due both to electron migration and lattice vibration, with the extent of each dependent on the specific material under observation.

An indication of the rate at which energy can be transferred by the diffusion process is given by the transport property of thermal conductivity. With a non-metal, the regularity of lattice arrangement has a very strong effect on the material's ability to conduct heat. For instance, quartz and diamond are two materials with a highly ordered crystalline structure. Consequently, each is able to conduct heat effectively. On the other hand, a glass such as fused silica is amorphous in nature and consists of a highly unordered lattice structure. These materials are inherently poor thermal conductors, and are characterized with low thermal conductivities. Fused silica is the

material used to explore the experimental method devised in the following chapters of this work.

The transport property of thermal diffusivity is also found in heat transfer analysis on a regular basis. This property is used to provide a measure of a material's ability to conduct thermal energy relative to its ability to store thermal energy. Thermal diffusivity is defined specifically as the ratio between a material's thermal conductivity (k) and volumetric heat capacity (ρC_p), where mass density is given by ρ. The volumetric heat capacity is a measure of a material's ability to store thermal energy on a 'per unit volume' basis, where the specific heat is a measure of a material's ability to store energy on a 'per unit mass' basis. Hence, a material with a large thermal diffusivity will respond quickly to changes in its thermal environment, and one characterized by a small thermal diffusivity will respond slower to the same changes.

When accurate thermal characterization of a material is desired, it is often necessary to obtain experimental data that allows for extraction of the property (or properties) of interest. This can be accomplished by using one of many techniques already available, or by devising a new or modified measurement method. In any case, the technique applied will likely involve determination of thermal conductivity or thermal diffusivity. Thermal conductivity measurements are not only difficult, but are time consuming since steady-state conditions are required. One key difficulty arises with energy loss at elevated temperatures. Radiation effects may be significant at such temperatures and must be properly accounted for.

The shortcomings in conductivity methods have led to a dramatic shift towards determination of transport properties using methods involving thermal diffusivity instead.[5] Because steady conditions are not a requirement, these techniques are much faster than their counterpart. In most cases, radiation losses can be easily accounted for and are sometimes neglected altogether. Once a diffusivity value has been determined, thermal conductivity can be readily calculated using knowledge of specific heat and mass density. However, it is important to recognize that if this route is taken to determine thermal conductivity, accurate specific heat data must be used in

the calculations or the resulting conductivity will likely be erroneous. Because of the shift toward diffusivity methods, only they will be further discussed in the paragraphs to follow.

An extensive number of measurement techniques have been developed for determining thin film properties. Lambropoulos *et al.*[2,3] have given a thorough review of various techniques and have also shown the effect of different system variables on the thermal properties of dielectric materials. Cahill *et al.*[6] have also presented several methods that are applicable to thin film property measurement over a range of thicknesses. Each of these papers provides valuable reference information on the measurement of thin film thermal properties.

DeVecchio *et al.*[7] have developed a phase sensitive technique for determining diffusivity of highly conductive samples. In their method, periodic heating is applied to one side of the sample and temperature response is measured at the other. The technique has been tested on glass, copper, and diamond, and properties resulting from its use are applicable in a direction perpendicular to the sample (through the thickness of the film). Chen and Tien[8] have demonstrated a method that allows for diffusivity measurements in both the perpendicular and parallel directions to a sample's surface. This technique is also phase sensitive where periodic heating is used to initiate thermal waves in the material and temperature response is measured at a particular location. Zhang and Grigoropoulos[9] have used silicon nitride films to demonstrate phase, amplitude, and heat pulse methods. A 3ω/decay technique studied by Frank *et al.*[10], where thermal diffusivity and effusivity can both be determined, has also been described in the literature.

The photoacoustic effect has been used to determine various characteristics of solid materials. The basic technique involves placing a layered structure inside an enclosed chamber filled with gas. A photoacoustic signal is generated as radiant energy (periodic) is absorbed by the structure. The absorbed energy causes the surface temperature of the structure to rise, thereby producing a localized variation in gas pressure at that surface. The acoustic signal is a product of the pressure variation at the front surface, and the signal's magnitude is proportional to the amount of heat

emanating from the solid absorber. If properly analyzed, the acoustic signal can supply important information relative to material properties of the solid structure.

Bennett and Patty[11] have suggested a technique for extracting thermal information from a photoacoustic signal and have also presented experimental measurements that illustrate the technique's use. Charpentier *et al.*[12] have used the photoacoustic effect for determining the thermal diffusivity of various metals. A method allowing for independent measurement of thermal conductivity and thermal diffusivity was presented by Swimm[13], and a technique presented by Lachaine and Poulet[14] allowed for determination of thermal diffusivity and effusivity of a thin polyester film using amplitude and phase information from a photoacoustic signal. It should be noted that all of the photoacoustic techniques discussed above are related to pioneering work by Rosencwaig and Gersho[15] who introduced the theory of the photoacoustic effect in solids.

The method presented in the following chapters is similar in theory to the photoacoustic techniques discussed above. However, appreciable differences can be found in the experimental apparatus required. For one, radiant energy is not used as a means for applying heat to the structure. Instead, a periodic voltage is applied across a resistive element to produce an I^2R heating effect. The resistive element is deposited on the structure's front surface. The new method also differs in how the surface temperature is measured. The photoacoustic techniques do not require direct measurement of surface temperature. Instead, a microphone is used to detect the acoustic signal resulting from temperature variations at the surface. A more direct approach is taken in the present method, where temperature characteristics are obtained with an infrared detector. Therefore, a gaseous chamber is not needed in the new method. As frequency dependent characteristics of the temperature response are obtained, it is possible to determine thermal properties of the thin film being studied.

3. THEORY

Two analytical models are developed in this chapter, both of which contain a periodic boundary condition as the driving force for heat conduction. Each model is based on a rectilinear coordinate system and the temperature response is sought at the same location that the periodic boundary condition is applied, namely at x=0. Underlying assumptions used for model development are also presented along with a description on how the analytical models are used in conjunction with measured data.

An important step in an analytical solution of any heat conduction problem is to present the differential equation of heat conduction in a form that suits each region of interest. For three-dimensional, time dependent heat conduction with volumetric heat generation (g), the temperature field (T) is given by,

$$\frac{\partial}{\partial x}\left(k\frac{\partial T}{\partial x}\right)+\frac{\partial}{\partial y}\left(k\frac{\partial T}{\partial y}\right)+\frac{\partial}{\partial z}\left(k\frac{\partial T}{\partial z}\right)+g=\rho C_p\frac{\partial T}{\partial t} \tag{3.1}$$

The spatial dimensions in this equation are (x, y, z), and time is represented by (t). Also, the region is composed of a material having thermal conductivity (k), density (ρ), and specific heat (C_p). This equation can be greatly simplified if appropriate assumptions are made. For both models developed in this chapter, it is assumed that heat conduction only takes place in a direction perpendicular to the surface exposed to heating. In other words, a one-dimensional form of Eq. (3.1) is used with (x) as the spatial coordinate. The thermal properties are also considered constant, and the volumetric energy generation within the solid is zero. With these assumptions, Eq. (3.1) reduces to,

$$\frac{\partial^2 T}{\partial x^2}=\frac{1}{\alpha}\frac{\partial T}{\partial t} \tag{3.2}$$

where (α) is the thermal diffusivity of the material and is defined by $\alpha = k/\rho C_p$.

There are numerous techniques available for obtaining a solution to this differential equation. A decision on choosing a technique may depend on many things, but it is usually driven by the type and complexity of the boundary conditions.

When a periodic boundary condition is present, analysis commonly results in a periodic sustained solution summed with a transient solution that decays to zero with time. If the transient part of the complete solution is of no interest, the problem becomes much easier to deal with and can be solved by a method known as complex combination. This method is used to obtain analytical results for both models in this chapter. Because this technique involves a few variable changes, care must be taken to keep the formulation of equations free of errors. In order to accomplish this, an outline given by Meyers[16] has proved very useful. A similar procedure is given below, where (x) represents a spatial coordinate and (θ) represents time. The use of complex temperatures is also illustrated by Arpaci.[17]

If $T(x, \theta)$ is the solution to the problem of interest, where a periodic disturbance $\sin(\omega\theta)$ or $\cos(\omega\theta)$ is imposed, then:

(1) Construct an identical problem for $S(x, \theta)$ by replacing the periodic disturbance of the 'T' problem with a disturbance that is shifted 90° in phase. For example, if the disturbance in the 'T' problem is $\sin(\omega\theta)$, then use a disturbance of $\cos(\omega\theta)$ in the 'S' problem.

(2) Construct a problem of the form $W(x, \theta) = T(x, \theta) + iS(x, \theta)$ by multiplying the 'S' problem by $i = \sqrt{-1}$ and adding the result to the 'T' problem.

(3) Assume a periodic product solution $W(x, \theta) = \Psi(x) \cdot e^{\pm i\omega\theta}$ to the 'W' problem. When this solution is inserted into the 'W' problem, (θ) will be eliminated entirely.

(4) Solve the resulting 'Ψ' problem for $\Psi(x)$.

(5) Write the solution $W(x, \theta) = \Psi(x) \cdot e^{\pm i\omega\theta}$ as the sum of real and imaginary parts, recognizing that the real component is $T(x, \theta)$, the sought after solution to the 'T' problem, and the imaginary component is the solution to the 'S' problem.

The resulting solution for the temperature distribution $T(x, \theta)$ will not be of a nature that is truly steady state. However, it can be viewed as pseudo-steady state due to its definite periodicity. It must be recognized that in order to use this solution technique, the entire problem must be homogeneous except for the periodic disturbance.

3.1. Analytical Models

The first model examines a single layer that is exposed to periodic heating at its front surface. The physical situation being modeled is that of I^2R heating imposed on the surface of a glass slide. A current flow is produced as a periodic voltage is applied across a thin (50 nm) nichrome strip that is deposited on the slide's surface. The current, which is also periodic in nature, produces the heating signal at the surface. In actuality, two layers exist. However, because the strip is thin and its thermal conductivity is very large compared to that of the slide, its physical dimensions are neglected in the analytical model altogether. Also, the slide is assumed thermally thick. Thus, periodic heating at the front surface is not expected to produce a periodic response at the back. This permits the use of a semi-infinite medium in the model which simplifies the analysis greatly. Results of this model are used to correct sample data obtained in the actual experiment, as explained later.

The second model examines a two layered structure, also with its front surface exposed to periodic heating. In this model, the layer upon which heat is applied represents the thin film sample under study, and the back layer is a substrate. The substrate is considered thermally thick, again permitting the use of a semi-infinite domain in the model.

The results of each model provide the temperature response at the front surface, from which a relationship for phase shift is ultimately extracted. The phase relationship is used for fitting experimental data using non-linear regression analysis.

3.1.1. One Domain

An elementary solution arises when a single semi-infinite domain with periodic surface heating is analyzed. This case is studied in order to show the basic technique of complex combination, and to provide an indication as to what can be expected in terms of results to a problem where a periodic heat source is present.

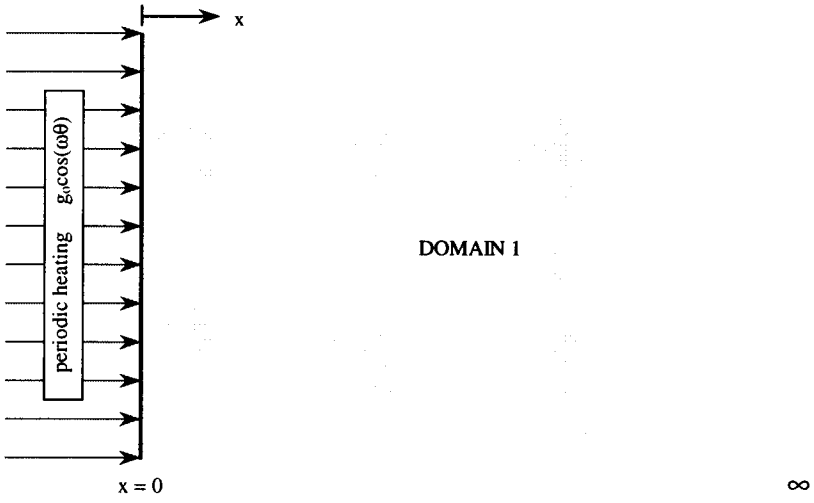

Figure 3.1 Single Domain Model

The first step toward obtaining an analytical solution to any heat conduction problem is to present the differential equation of heat conduction in a form that suits the region of interest. As stated previously, one-dimensional conduction with constant properties and zero energy generation is assumed for the following analysis. The equation governing conduction in the region of domain 1 is expressed as,

$$\frac{\partial^2 T}{\partial x^2} = \frac{1}{\alpha}\frac{\partial T}{\partial \theta} \tag{3.3}$$

where (T) is the temperature within the region , (θ) represents time, and (α) is the thermal diffusivity of the material composing the region. This equation is of second

order in the spatial coordinate (x), and first order in the time coordinate (θ). Thus, to obtain a full solution for the temperature distribution $T(x, \theta)$ within the solid, two boundary conditions and one initial condition are required.

As periodic heating is applied to the surface, the solid is expected to reach a 'baseline', or mean temperature. The periodic response will fluctuate about this value. For simplicity, the mean temperature and initial temperature are considered equal and are given a value of zero. Therefore, the initial condition is stated mathematically as $T(x, 0)=0$.

At the front surface ($x=0$), the periodic heat source is expressed analytically as a boundary condition of the form,

$$q''(0, \theta) = -k \left.\frac{\partial T}{\partial x}\right|_{x=0} = g_o \cos(\omega\theta) \tag{3.4}$$

The second boundary condition is imposed at a position far removed from the periodic heat source where the thermal waves travelling through the solid have been completely dampened. There will be no thermal gradient at this location, such that the temperature will be equal to the initial temperature of the solid,

$$T(x \to \infty, \theta) = 0 \tag{3.5}$$

Looking back at the outline given for the method of complex combination, it is clear that the mathematical description of the 'T' problem is complete.

Now, as step one of the outline suggests, an identical problem is constructed ('S' problem). However, the periodic heat source is replaced by a source that is 90° out of phase with that of the 'T' problem. In doing this, the differential equation governing heat conduction in domain 1 of the 'S' problem becomes,

$$\frac{\partial^2 S}{\partial x^2} = \frac{1}{\alpha}\frac{\partial S}{\partial \theta} \tag{3.6}$$

The initial condition for this problem is that the entire region is at a constant temperature, and is equal to S(x, 0)=0. Upon transformation, the boundary conditions for the 'S' problem become,

$$q''(0,\theta) = -k\left.\frac{\partial S}{\partial x}\right|_{x=0} = g_o \sin(\omega\theta) \tag{3.7}$$

$$S(x \to \infty, \theta) = 0 \tag{3.8}$$

The second step in this method of solution results in the 'W' problem and is accomplished by forming the complex combination W=T+iS. After appropriate derivatives are taken and substitutions made, the differential equation for domain 1 of the 'W' problem becomes,

$$\frac{\partial^2 W}{\partial x^2} = \frac{1}{\alpha}\frac{\partial W}{\partial \theta} \rightarrow \frac{\partial^2 T}{\partial x^2} + i\frac{\partial^2 S}{\partial x^2} = \frac{1}{\alpha}\left[\frac{\partial T}{\partial \theta} + i\frac{\partial S}{\partial \theta}\right] \tag{3.9}$$

and boundary conditions transform into,

$$q''(0,\theta) = -k\left.\frac{\partial W}{\partial x}\right|_{x=0} = g_o\, e^{i\omega\theta} \tag{3.10}$$

$$W(x \to \infty, \theta) = 0 \tag{3.11}$$

In Eq. (3.10), the complex relationship $e^{i\omega\theta}=\cos(\omega\theta)+i\sin(\omega\theta)$ is used for simplification. Again, the solution for temperature in the entire region is equal to zero prior to heating, which is stated as W=0.

As the third step suggests, a periodic product solution to the 'W' problem is assumed. This solution takes the form $W(x, \theta) = \Psi(x)\cdot e^{i\omega\theta}$ and should be substituted into Eq. (3.9). In order to apply this solution, the following derivatives become useful.

$$\frac{\partial W}{\partial x} = \frac{d\Psi}{dx} e^{i\omega\theta} \tag{3.12}$$

$$\frac{\partial^2 W}{\partial x^2} = \frac{d^2\Psi}{dx^2} e^{i\omega\theta} \tag{3.13}$$

$$\frac{\partial W}{\partial \theta} = i\omega \Psi e^{i\omega\theta} \tag{3.14}$$

These relationships are substituted directly into Eq. (3.9), yielding the new differential equation,

$$\frac{\partial^2 W}{\partial x^2} = \frac{1}{\alpha}\frac{\partial W}{\partial \theta} \rightarrow e^{i\omega\theta}\frac{d^2\Psi}{dx^2} = \frac{i\omega}{\alpha} e^{i\omega\theta}\Psi \tag{3.15}$$

The exponential terms of Eq. (3.15) conveniently cancel, resulting in a differential equation where time is no longer involved. Therefore, an initial condition is not needed to obtain a solution to this equation. However, boundary conditions are required. After canceling like terms, Eq. (3.15) is rearranged into,

$$\frac{d^2\Psi}{dx^2} - \frac{i\omega}{\alpha}\Psi = 0 \tag{3.16}$$

whose boundary conditions are,

$$q''(0) = -k\left.\frac{d\Psi}{dx}\right|_{x=0} = g_o \tag{3.17}$$

$$\Psi(x \rightarrow \infty) = 0 \tag{3.18}$$

Now step three is complete, and the new 'Ψ' problem is solved for $\Psi(x)$. Equation (3.16) is a linear, homogeneous differential equation for which a well-known solution exists. One form of this solution is commonly expressed as,

$$\Psi = A e^{-\sqrt{\frac{i\omega}{\alpha}}x} + B e^{\sqrt{\frac{i\omega}{\alpha}}x} \tag{3.19}$$

This general solution has two unknown constants of integration, so each boundary condition for the 'Ψ' problem is utilized. Before doing so, the equation is placed in another form using standard rules for manipulation of complex variables,

$$\Psi = A e^{-\sqrt{\frac{\omega}{2\alpha}}x} e^{-i\sqrt{\frac{\omega}{2\alpha}}x} + B e^{\sqrt{\frac{\omega}{2\alpha}}x} e^{i\sqrt{\frac{\omega}{2\alpha}}x} \tag{3.20}$$

Now the boundary condition given by Eq. (3.18) is applied. As x becomes very large, the solution does not remain finite. In order to produce a solution valid at all x locations, the B constant is set to zero. This reduces the solution to,

$$\Psi = A e^{-\sqrt{\frac{\omega}{2\alpha}}x} e^{-i\sqrt{\frac{\omega}{2\alpha}}x} \tag{3.21}$$

In order to apply the periodic boundary condition at the front surface, the derivative of Eq. (3.21) is needed,

$$\frac{d\Psi}{dx} = -A\sqrt{\frac{i\omega}{\alpha}} e^{-i\sqrt{\frac{\omega}{2\alpha}}x} \tag{3.22}$$

Upon setting x=0 in this derivative and applying the boundary condition of Eq. (3.17), the constant A becomes,

$$A = \frac{g_o}{k}\sqrt{\frac{\alpha}{i\omega}} \tag{3.23}$$

The complete solution to the 'Ψ' problem takes the form of,

$$\Psi = \frac{g_o}{k}\sqrt{\frac{\alpha}{\omega}}\frac{1}{\sqrt{i}} e^{-\sqrt{\frac{i\omega}{\alpha}}x} \tag{3.24}$$

which can be simplified using rules of complex variables to,

$$\Psi = \frac{g_o}{k}\sqrt{\frac{\alpha}{\omega}}\, e^{-i\frac{\pi}{4}}\, e^{-\sqrt{\frac{\omega}{2\alpha}}x}\, e^{-i\sqrt{\frac{\omega}{2\alpha}}x} \tag{3.25}$$

Moving on to the fifth and final step as depicted by the outline for complex combination, the solution to the 'W' problem is reconstructed into $W(x, \theta)=\Psi(x)\cdot e^{i\omega\theta}$,

$$W = \frac{g_o}{k}\sqrt{\frac{\alpha}{\omega}}\, e^{-i\frac{\pi}{4}}\, e^{-\sqrt{\frac{\omega}{2\alpha}}x}\, e^{-i\sqrt{\frac{\omega}{2\alpha}}x}\, e^{i\omega\theta} \tag{3.26}$$

Equation (3.26) is now broken into a real component and imaginary component. It is recognized that the imaginary component is the complete solution to the 'S' problem, which is no longer of interest. However, the real component of Eq. (3.26) is valuable. This part is the solution to the 'T' problem which yields the sought-after temperature response of the solid. The full solution for the temperature distribution in the semi-infinite medium with boundary and initial conditions presented is now stated as,

$$T = \frac{g_o}{k}\sqrt{\frac{\alpha}{\omega}}\, e^{-\sqrt{\frac{\omega}{2\alpha}}x}\, \cos\left(\omega\theta - \sqrt{\frac{\omega}{2\alpha}}\, x - \frac{\pi}{4}\right) \tag{3.27}$$

A few key points are evident in this solution. First of all, the amplitude of the temperature response at the front surface is not only a function of surface heating strength, but also of two material properties and heating frequency. As expected, the amplitude of the temperature response decreases with increasing frequency and also decays with depth from the front surface. If a thermal diffusion length[15] is defined as,

$$\mu = \sqrt{\frac{2\alpha}{\omega}} \tag{3.28}$$

then Eq. (3.27) becomes,

$$T = \frac{g_o}{k}\sqrt{\frac{\alpha}{\omega}}\, e^{-\frac{x}{\mu}}\, \cos\left(\omega\theta - \frac{x}{\mu} - \frac{\pi}{4}\right) \tag{3.29}$$

This equation is examined to show the rapid amplitude attenuation of the temperature response as depth from the front surface of the solid increases. As shown in Fig. (3.2), at a distance of only 2π times the thermal diffusion length, variation in the periodic temperature is effectively zero.

As stated previously, the one domain model represents periodic heating applied to the surface of a glass slide. If the values $\alpha=8.34\text{x}10^{-7}$ m^2/s and $\omega=2\pi500$ are inserted into Eq. (3.28), the thermal diffusion length becomes $\mu=2.30\text{x}10^{-5}$ m. When multiplied by 2π, the distance into the solid becomes $1.45\text{x}10^{-4}$ m. The values used to obtain diffusion length are those for thermal diffusivity of fused silica at room temperature and a heating frequency of 500 Hz, respectively. The calculation shows that use of a standard 1 mm ($1.0\text{x}10^{-3}$ m) thick slide of fused silica is sufficient to ensure that the thermally thick assumption will be met for any frequency in excess of 500 Hz.

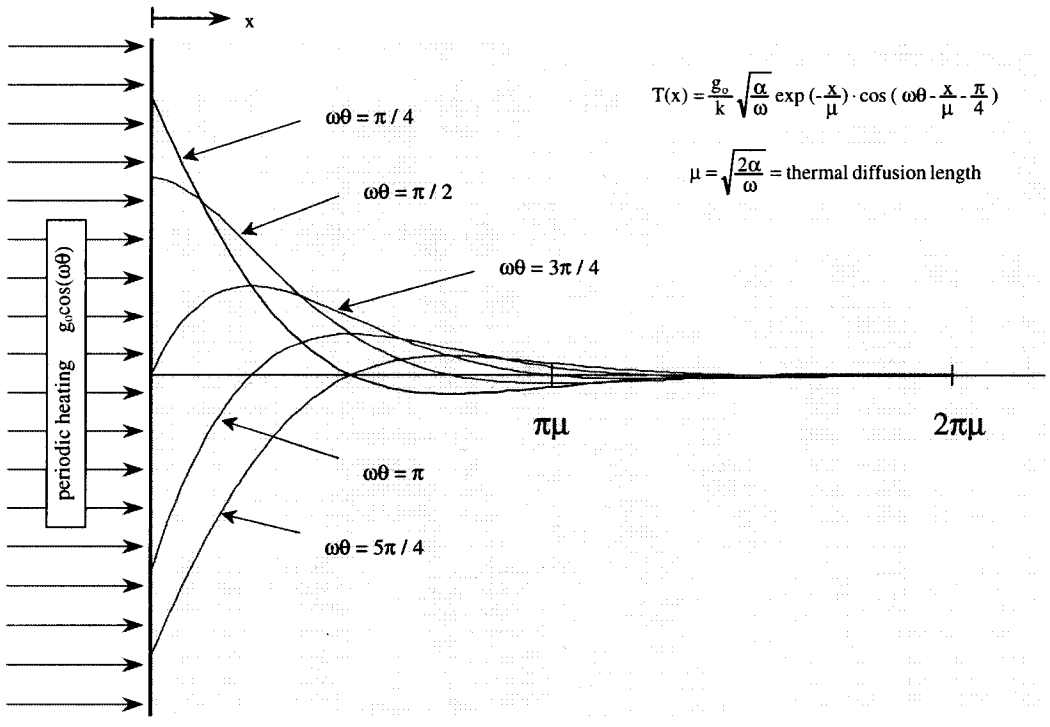

Figure 3.2 Time Dependent Temperature Distribution In Domain 1

Of more importance is the phase shift between the temperature response of the medium and the periodic heating signal. Within the solid, phase shift is dependent on both frequency and material properties. However, at the front surface it reduces to a constant value. The desired solution for the temperature response at x=0 simplifies to,

$$T = \frac{g_o}{k}\sqrt{\frac{\alpha}{\omega}}\cos\left(\omega\theta - \frac{\pi}{4}\right) \tag{3.30}$$

This equation clearly shows that for a one dimensional, semi-infinite region exposed to periodic heating, the temperature response of the surface will lag the heating signal by a value of 45° regardless of material properties and heating frequency.

3.1.2. Two Domain

In the thin film situation of interest, a multi-layered structure exists. This complicates problem analysis somewhat, but a closed form solution is still attainable. The physical situation is modeled as a two layered structure with the surface at x=0 exposed to periodic heating. Here, domain 1 is the thin film and domain 2 is a thermally thick silicon substrate. To produce periodic heating, a thin nichrome strip is physically present at the x=0 surface. This gives a situation in which three layers exist. However, because the nichrome strip is very thin (50 nm) and highly conductive as compared to the thin film, it is neglected in this analytical model.

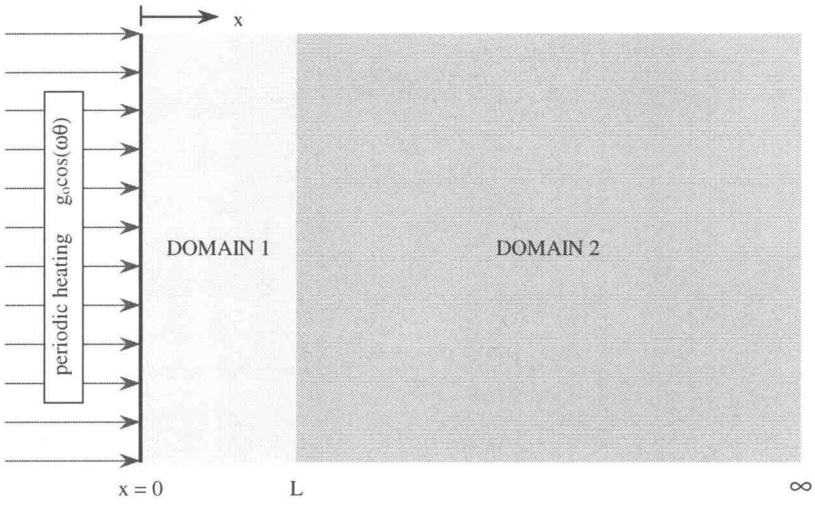

Figure 3.3 Two Domain Model

As the outline for complex combination suggests, a mathematical description of the 'T' problem is first needed. This 'T' problem is fully characterized by a set of governing differential equations and corresponding initial and boundary conditions. The equations governing the inner regions of each domain of the 'T' problem are stated as,

$$\frac{\partial^2 T_1}{\partial x^2} = \frac{1}{\alpha_1}\frac{\partial T_1}{\partial \theta} \tag{3.31}$$

$$\frac{\partial^2 T_2}{\partial x^2} = \frac{1}{\alpha_2}\frac{\partial T_2}{\partial \theta} \tag{3.32}$$

Each of the above equations is of second order in the spatial coordinate (x), and of first order in the time coordinate (θ). Thus, two boundary conditions and one initial condition must accompany each equation in order to describe the physical situation in full. Similar to the previous model, initial conditions state that temperature is equal to zero throughout both regions prior to heating. These initial conditions are not carried through the following analysis, but are implied.

At the front surface of domain 1 (x=0), a periodic heat flux is being applied. This boundary condition is stated mathematically as,

$$q''(0,\theta) = -k_1 \left.\frac{\partial T_1}{\partial x}\right|_{x=0} = g_o \cos(\omega\theta) \tag{3.33}$$

On the other side of domain 1 (x=L), the second boundary condition is formed. By using energy considerations at this location it becomes apparent that the heat flux leaving the back surface of domain 1 must be equal to the heat flux entering the front surface of domain 2. This is stated as,

$$-k_1 \left.\frac{\partial T_1}{\partial x}\right|_{x=L} = -k_2 \left.\frac{\partial T_2}{\partial x}\right|_{x=L} \tag{3.34}$$

If it is assumed that superior thermal contact exists between domain 1 and domain 2, then it is permissible to neglect thermal resistance between the two. Therefore, a temperature jump will not exist across the interface,

$$T_1(L,\theta) = T_2(L,\theta) \tag{3.35}$$

Finally, as the spatial coordinate (x) increases to values much larger than L, the magnitude of the periodic temperature response felt at that location due to the application of heat at the structures front surface decreases. For very large values of x, the thermal wave has completely dampened such that,

$$T_2(x \to \infty, \theta) = 0 \tag{3.36}$$

In order to solve the problem for T(x, θ), the steps previously outlined for complex combination are followed. First, a 'S' problem is formulated that is similar to the 'T' problem, but with a periodic disturbance that has been altered. In doing this, the 'S' problem becomes,

$$\frac{\partial^2 S_1}{\partial x^2} = \frac{1}{\alpha_1}\frac{\partial S_1}{\partial \theta} \tag{3.37}$$

$$\frac{\partial^2 S_2}{\partial x^2} = \frac{1}{\alpha_2}\frac{\partial S_2}{\partial \theta} \tag{3.38}$$

Each of the boundary conditions corresponding to these two new 'S' problems remain unchanged, except for a variable change and the replacement of the periodic boundary condition $g_o\cos(\omega\theta)$ with the new condition $g_o\sin(\omega\theta)$. In doing this, the four boundary conditions become,

$$x = 0 \qquad q'' = -k_1 \left.\frac{\partial S_1}{\partial x}\right|_{x=0} = g_o \sin(\omega\theta) \tag{3.39}$$

$$x = L \qquad -k_1 \left.\frac{\partial S_1}{\partial x}\right|_{x=L} = -k_2 \left.\frac{\partial S_2}{\partial x}\right|_{x=L} \tag{3.40}$$

$$x = L \qquad S_1 = S_2 \tag{3.41}$$

$$x \to \infty \qquad S_2 = 0 \tag{3.42}$$

By following step 2 of the outline, the 'W' problem (W=T+iS) is put together. Upon differentiation and substitution, the governing equations for each domain of the 'W' problem become,

$$\frac{\partial^2 W_1}{\partial x^2} = \frac{1}{\alpha_1}\frac{\partial W_1}{\partial \theta} \quad \rightarrow \quad \frac{\partial^2 T_1}{\partial x^2} + i\frac{\partial^2 S_1}{\partial x^2} = \frac{1}{\alpha_1}\left[\frac{\partial T_1}{\partial \theta} + i\frac{\partial S_1}{\partial \theta}\right] \tag{3.43}$$

$$\frac{\partial^2 W_2}{\partial x^2} = \frac{1}{\alpha_2}\frac{\partial W_2}{\partial \theta} \quad \rightarrow \quad \frac{\partial^2 T_2}{\partial x^2} + i\frac{\partial^2 S_2}{\partial x^2} = \frac{1}{\alpha_2}\left[\frac{\partial T_2}{\partial \theta} + i\frac{\partial S_2}{\partial \theta}\right] \tag{3.44}$$

with boundary conditions,

$$x = 0 \qquad q'' = -k_1 \left.\frac{\partial W_1}{\partial x}\right|_{x=0} = g_o e^{i\omega\theta} \tag{3.45}$$

$$x = L \qquad -k_1 \left.\frac{\partial W_1}{\partial x}\right|_{x=L} = -k_2 \left.\frac{\partial W_2}{\partial x}\right|_{x=L} \tag{3.46}$$

$$x = L \qquad W_1 = W_2 \tag{3.47}$$

$$x \to \infty \qquad W_2 = 0 \tag{3.48}$$

The 'W' problem is solved by applying all of the boundary conditions presented above. A solution is assumed that takes the form $W(x, \theta)=\Psi(x)\cdot e^{i\omega\theta}$. After differentiation and substitution of this solution, the problem becomes,

$$\frac{\partial^2 W_1}{\partial x^2} = \frac{1}{\alpha_1}\frac{\partial W_1}{\partial \theta} \rightarrow e^{i\omega\theta}\frac{d^2\Psi_1}{dx^2} = \frac{i\omega}{\alpha_1} e^{i\omega\theta}\Psi_1 \tag{3.49}$$

$$\frac{\partial^2 W_2}{\partial x^2} = \frac{1}{\alpha_2}\frac{\partial W_2}{\partial \theta} \rightarrow e^{i\omega\theta}\frac{d^2\Psi_2}{dx^2} = \frac{i\omega}{\alpha_2} e^{i\omega\theta}\Psi_2 \tag{3.50}$$

After examining the transformations, it becomes apparent that all terms involving θ cancel, reducing the problem to one that is only spatially dependent. Remaining are two problems involving only $\Psi(x)$ whose complete formulations are,

$$\frac{d^2\Psi_1}{dx^2} - \frac{i\omega}{\alpha_1}\Psi_1 = 0 \tag{3.51}$$

$$\frac{d^2\Psi_2}{dx^2} - \frac{i\omega}{\alpha_2}\Psi_2 = 0 \tag{3.52}$$

Similar to previous transformations, the four boundary conditions for this set of differential equations are stated as,

$$x = 0 \qquad \left.\frac{d\Psi_1}{dx}\right|_{x=0} = -\frac{g_o}{k_1} \tag{3.53}$$

$$x = L \qquad -k_1 \left.\frac{d\Psi_1}{dx}\right|_{x=L} = -k_2 \left.\frac{d\Psi_2}{dx}\right|_{x=L} \tag{3.54}$$

$$x \to \infty \qquad \Psi_2 = 0 \tag{3.55}$$

$$x = L \qquad \Psi_1 = \Psi_2 \tag{3.56}$$

The problem as stated above is linear and homogeneous. A well known solution exists for both Ψ_1 and Ψ_2, and is commonly expressed in the form,

$$\Psi_1 = A_1 e^{-\sqrt{\frac{i\omega}{\alpha_1}}x} + B_1 e^{\sqrt{\frac{i\omega}{\alpha_1}}x} \tag{3.57}$$

$$\Psi_2 = A_2 e^{-\sqrt{\frac{i\omega}{\alpha_2}}x} + B_2 e^{\sqrt{\frac{i\omega}{\alpha_2}}x} \tag{3.58}$$

Now, the equations for Ψ_1 and Ψ_2 must be solved. There are a total of four unknown constants (A_1, B_1, A_2, B_2) within the system of equations. In order to solve the equations, all four boundary conditions need to be applied. First, Eq. (3.58) is manipulated using standard rules for complex quantities into,

$$\Psi_2 = A_2 e^{-\sqrt{\frac{\omega}{2\alpha_2}}x} e^{-i\sqrt{\frac{\omega}{2\alpha_2}}x} + B_2 e^{\sqrt{\frac{\omega}{2\alpha_2}}x} e^{i\sqrt{\frac{\omega}{2\alpha_2}}x} \tag{3.59}$$

Upon application of boundary condition (3.55) with x tending toward very large values, Ψ_2 does not remain bounded due to the positive (real) exponential term of Eq. (3.59). Therefore, B_2 is set to zero producing a solution valid at all x locations.

In order to apply boundary condition (3.53), the derivative of Eq. (3.57) is first obtained. The resulting derivative is expressed as,

$$\frac{d\Psi_1}{dx} = - A_1 \sqrt{\frac{i\omega}{\alpha_1}}\, e^{-\sqrt{\frac{i\omega}{\alpha_1}}x} + B_1 \sqrt{\frac{i\omega}{\alpha_1}}\, e^{\sqrt{\frac{i\omega}{\alpha_1}}x} \tag{3.60}$$

which at x=0 becomes,

$$\left.\frac{d\Psi_1}{dx}\right|_{x=0} = \sqrt{\frac{i\omega}{\alpha_1}}\,(B_1 - A_1) \tag{3.61}$$

Equation (3.61) and boundary condition (3.53) are now combined. When this is done, the constant B_1 is solved for in terms of A_1,

$$B_1 = A_1 - \frac{g_o}{k_1}\sqrt{\frac{\alpha_1}{i\omega}} \tag{3.62}$$

It is apparent that the complex term $i\omega/\alpha$ is showing up quite often. In order to simplify the remaining derivation, the following complex variables are defined,

$$\xi_1 = \sqrt{\frac{i\omega}{\alpha_1}} \tag{3.63}$$

$$\xi_2 = \sqrt{\frac{i\omega}{\alpha_2}} \tag{3.64}$$

Upon substituting results for B_1 and B_2, and utilizing each new complex quantity as defined above, the solutions for Ψ_1 and Ψ_2 become much more manageable,

$$\Psi_1 = A_1\, e^{-\xi_1 x} + (A_1 - \frac{g_o}{k_1\,\xi_1})\, e^{\xi_1 x} \tag{3.65}$$

$$\Psi_2 = A_2\, e^{-\xi_2 x} \tag{3.66}$$

Next, each solution is differentiated to enable application of condition (3.54) at the interface (x=L). After doing this, the spatial term is set to x=L resulting in equations of the form,

$$\left.\frac{d\Psi_1}{dx}\right|_{x=L} = (A_1\xi_1 - \frac{g_o}{k_1})e^{\xi_1 L} - A_1\xi_1 e^{-\xi_1 L} \tag{3.67}$$

$$\left.\frac{d\Psi_2}{dx}\right|_{x=L} = -A_2\xi_2 e^{-\xi_2 L} \tag{3.68}$$

Now, substitution of each derivative into the x=L boundary condition gives,

$$(A_1\xi_1 - \frac{g_o}{k_1})e^{\xi_1 L} - A_1\xi_1 e^{-\xi_1 L} = -\frac{k_2}{k_1}A_2\xi_2 e^{-\xi_2 L} \tag{3.69}$$

After mathematical manipulation of Eq. (3.69), the constant A_2 is solved for directly. This results in,

$$A_2 = A_1\frac{k_1\xi_1}{k_2\xi_2}\left[e^{L(\xi_2-\xi_1)} - e^{L(\xi_2+\xi_1)}\right] + \frac{g_o}{k_2\xi_2}e^{L(\xi_2+\xi_1)} \tag{3.70}$$

The only unknown constant remaining in the system of equations is A_1. The final boundary condition (3.56) is utilized to solve for this constant. In order to apply the boundary condition, A_2 is substituted into the solution for Ψ_2 given by Eq. (3.66). Then the solutions for Ψ_1 and Ψ_2 are applied at x=L. In doing this, the solutions become,

$$\Psi_1(x=L) = A_1 e^{-\xi_1 L} + (A_1 - \frac{g_o}{k_1\xi_1})e^{\xi_1 L} \tag{3.71}$$

$$\Psi_2(x=L) = \left[A_1\frac{k_1\xi_1}{k_2\xi_2}\left[e^{L(\xi_2-\xi_1)} - e^{L(\xi_2+\xi_1)}\right] + \frac{g_o}{k_2\xi_2}e^{L(\xi_2+\xi_1)}\right]e^{-\xi_2 L} \tag{3.72}$$

Next, the exponential terms in Ψ_2 are combined to produce a much more manageable equation of the form,

$$\Psi_2(x=L) = A_1 \frac{k_1\xi_1}{k_2\xi_2}\left[e^{-\xi_1 L} - e^{\xi_1 L}\right] + \frac{g_o}{k_2\xi_2} e^{\xi_1 L} \tag{3.73}$$

Finally, the complex temperatures $\Psi_1(x=L)$ and $\Psi_2(x=L)$ are set equal to each other. Once this is done, an equation results in which the only unknown constant is A_1. Solving for this constant produces,

$$A_1 = \frac{g_o\, e^{\xi_1 L}\left(\frac{k_2\xi_2}{k_1\xi_1} + 1\right)}{(k_2\xi_2 + k_1\xi_1)e^{\xi_1 L} + (k_2\xi_2 - k_1\xi_1)e^{-\xi_1 L}} \tag{3.74}$$

Now that complete solutions for both complex temperatures Ψ_1 (domain 1) and Ψ_2 (domain 2) have been formulated, the spatial location of real interest is examined. This location is at the front surface (x=0). After substitution of x=0 into Eq. (3.65), the solution at the front surface becomes,

$$\Psi_1(x=0) = 2A_1 - \frac{g_o}{k_1\xi_1} \tag{3.75}$$

After the solution for the constant A_1 is placed into Eq. (3.75), the equation is manipulated to yield,

$$\Psi_1(x=0) = \frac{2g_o}{k_1\xi_1}\left[\frac{1}{1+\left(\frac{k_2\xi_2 - k_1\xi_1}{k_2\xi_2 + k_1\xi_1}\right)e^{-2\xi_1 L}} - \frac{1}{2}\right] \tag{3.76}$$

Finally, this solution is used to reconstruct the 'W' problem. Similar to the one domain derivation of the previous section, a solution for $W_1(0, \theta)$ is sought that is

broken into a real component and an imaginary component. In order to accomplish this, a new term is first introduced. The effusivity of the materials of domain 1 and domain 2 are defined as,

$$e_1 = \sqrt{k_1 \rho_1 C_{p1}} = \frac{k_1}{\sqrt{\alpha_1}} \tag{3.77}$$

$$e_2 = \sqrt{k_2 \rho_2 C_{p2}} = \frac{k_2}{\sqrt{\alpha_2}} \tag{3.78}$$

If not recognized, the similarity between the appearance of effusivity (e_1) and all exponential terms (e) that are scattered throughout the previous equations can lead to difficulties in the problem solving process. In all equations formulated in the body of this text, an effusivity will possess a subscript and an exponential will not.

Effusivity as defined above is first utilized toward simplification of a term found in Eq. (3.76). The simplification takes the form,

$$\frac{k_2\xi_2 - k_1\xi_1}{k_2\xi_2 + k_1\xi_1} = \frac{k_2\sqrt{\frac{i\omega}{\alpha_2}} - k_1\sqrt{\frac{i\omega}{\alpha_1}}}{k_2\sqrt{\frac{i\omega}{\alpha_2}} + k_1\sqrt{\frac{i\omega}{\alpha_1}}} = \frac{e_2 - e_1}{e_2 + e_1} \tag{3.79}$$

Now, the complex term $k_1\xi_1$ still remains in Eq. (3.76) prior to the first set of brackets. This term is also simplified using the definition of effusivity. In doing so, the complete solution for the complex temperature Ψ_1 at the front surface (x=0) can be rearranged mathematically into,

$$\Psi_1 (x = 0) = \frac{g_o (1 - i)}{e_1\sqrt{2\omega}} \left[\frac{1 - \left(\frac{e_2 - e_1}{e_2 + e_1}\right) e^{-2\xi_1 L}}{1 + \left(\frac{e_2 - e_1}{e_2 + e_1}\right) e^{-2\xi_1 L}} \right] \tag{3.80}$$

By defining $E=(e_2-e_1)/(e_2+e_1)$, Eq. (3.80) is further reduced to,

$$\Psi_1(x=0)=\frac{g_o(1-i)}{e_1\sqrt{2\omega}}\left[\frac{1-Ee^{-2\xi_1 L}}{1+Ee^{-2\xi_1 L}}\right] \tag{3.81}$$

This expression is still relatively complicated due to the complex terms enclosed in brackets in both the numerator and denominator, along with the imaginary term outside of the brackets. With quite some effort, this equation is broken into real and imaginary components. The results of this mathematical reduction are presented in the form Ψ_1=REAL-iIMAG where,

$$\text{REAL}=\left(\frac{g_o}{e_1\sqrt{2\omega}}\right)\frac{1-e^{-2\Gamma}E^2+2Ee^{-\Gamma}\sin(\Gamma)}{1+e^{-2\Gamma}E^2+2Ee^{-\Gamma}\cos(\Gamma)} \tag{3.82}$$

$$\text{IMAG}=\left(\frac{g_o}{e_1\sqrt{2\omega}}\right)\frac{1-e^{-2\Gamma}E^2-2Ee^{-\Gamma}\sin(\Gamma)}{1+e^{-2\Gamma}E^2+2Ee^{-\Gamma}\cos(\Gamma)} \tag{3.83}$$

In both of the equations above, the following relationship has been substituted for purposes of simplification,

$$\Gamma=\sqrt{\frac{2\omega}{\alpha_1}}L \tag{3.84}$$

The solution is now in a form where reconstruction of the 'W' problem can be accomplished by following the same steps presented in the previous section during reconstruction of the 'W' problem for a single region exposed to periodic surface heating. After reconstruction, the 'W' problem is separated into a real component ('T' problem) and an imaginary component ('S' problem). In doing this, the temperature response at the front surface of a two layered structure $T(0, \theta)$ due to periodic heating at that structure's front surface is given by,

$$T=\text{MAG}\cdot\cos(\omega\theta-\phi) \tag{3.85}$$

where the amplitude and the phase shift of the temperature excursion are expressed as,

$$MAG = \frac{g_o}{e_1\sqrt{\omega}}\left(\frac{\sqrt{\left(1-e^{-2\Gamma}E^2\right)^2+4E^2e^{-2\Gamma}\sin^2(\Gamma)}}{1+e^{-2\Gamma}E^2+2Ee^{-\Gamma}\cos(\Gamma)}\right) \tag{3.86}$$

$$\phi = \text{atan}\left(\frac{1-e^{-2\Gamma}E^2-2Ee^{-\Gamma}\sin(\Gamma)}{1-e^{-2\Gamma}E^2+2Ee^{-\Gamma}\sin(\Gamma)}\right) \tag{3.87}$$

With the expression for phase shift as defined by Eqs. (3.85) and (3.87), a positive value for phase shift corresponds to a lag in temperature response with respect to the heating signal. Also note that the phase shift at the front surface is no longer a simple constant as was for the single domain model, but has become a complicated analytic expression.

3.2. Curve Fitting

The second model results in a phase shift dependent on five different quantities, three of which are embedded in the expression for Γ and two in the relationship for E. Of these five variables, three are considered known. The known values are the frequency of the periodic heat source ($\omega=2\pi f$), the film thickness (L), and also the effusivity of the silicon substrate (e_2). The heating frequency is controlled directly through the experimental apparatus, the film thickness is measured prior to testing, and the effusivity of silicon is calculated with temperature dependent properties using the relationship $e_2 = \sqrt{k_2 \rho_2 c_{p2}}$. This leaves the film's effusivity (e_1) and diffusivity (α_1) as unknown thermal properties to be obtained with experimental data produced by the measurement system. Once these two independent properties are known, the thin film's thermal conductivity and specific heat can readily be determined.

Before the curve fitting process can begin, accurate thermal property data for the silicon substrate is required. The density is held fixed at ρ_2=2330 kg/m^3 and the

thermal conductivity and specific heat are allowed to vary with temperature. A literature survey for conductivity of silicon as a function of temperature[18,19] has yielded a range of values with up to 10% uncertainty. Possible contributors to such variation are doping level and property measurement technique. It is known that the silicon substrate used in this experiment is of n-type, lightly doped with phosphorus ($10^{15}/cm^3$). Apparently, this material has not been 'well' characterized thermally. Therefore, thermal conductivity for high purity silicon is used for effusivity calculations.[19] The specific heat values used in property calculations are also those of single crystal silicon of high purity,[20] although similar variation was found.

All of the thermal properties of silicon used during curve fitting of experimental data are presented as a function of temperature in Table 3.1. To provide an idea of how the uncertainty in a single variable at a given temperature can effect the curve fitting results, two values of thermal conductivity are used. The nominal value of thermal conductivity ($k_{2\,(a)}$) is found on the left side of Table 3.1 and a corrective value ($k_{2\,(b)}$), obtained simply by subtracting 10 from the nominal value, is on the right.

Table 3.1 Selected Thermal Properties of Silicon

		Nominal		Corrective	
T (°C)	C_{p2} (J/kg K)	$k_{2\,(a)}$ (W/m K)	$e_{2\,(a)}$ (W $s^{1/2}$/K)	$k_{2\,(b)}$ (W/m K)	$e_{2\,(b)}$ (W $s^{1/2}$/K)
25	710.5	149.0	15706	139.0	15169
40	726.0	139.0	15334	129.0	14772
48.7	734.0	134.1	15144	124.1	14568
50	735.0	133.0	15092	123.0	14514
75	755.0	120.0	14529	110.0	13911
96	770.0	110.6	14086	100.6	13434
100	773.0	109.0	14011	99.0	13353
143.5	796.5	94.3	13229	84.3	12508
150	800.0	93.0	13166	83.0	12438
190.9	817.2	83.2	12586	73.2	11806
200	821.0	81.0	12448	71.0	11654
238.3	834.2	74.3	12017	64.3	11179
250	838.0	72.0	11857	62.0	11003
285.7	848.6	67.1	11518	57.1	10625
300	853.0	65.0	11366	55.0	10455

This provides two values of effusivity for use at each temperature during the curve fitting routine. The value of 10 was chosen for simplicity, and corresponds to a 7% reduction at room temperature and a 15% reduction at 300 K. To keep variables to a minimum, only one value of specific heat is used at each temperature. It is realized that uncertainty also exists in places other than the thermal conductivity of silicon. In consideration to this, a detailed uncertainty analysis is presented in the results section of this paper.

At the onset of this project, an iterative curve fitting process was anticipated requiring the use of both phase data and magnitude data as a function of frequency in order to obtain two independent thermal properties of the thin film. To do this, phase data would first be fit to the analytical model while assuming a value for one of the unknown thermal properties (effusivity). A value for the other unknown property (diffusivity) would result from the fitting routine. This diffusivity value would then be held constant in a fit of the magnitude data to its model, resulting in a value for effusivity. The new effusivity value would be used in another fit of the phase data to the phase model, producing yet another diffusivity value. The process would be repeated until the values converged, resulting in a diffusivity/effusivity pair that did not vary between fitting trials.

Through extensive use of this procedure it was determined that phase data at the front surface of the thin film sample is very rich in information content, such that it alone is all that is required. Because the data is a very strong function of diffusivity, a single fitting routine using only phase data is sufficient to produce the same results obtained by the previous approach. This routine involves a two-parameter fit using non-linear regression, without the difficulties inherent in the iterative approach. In this method, phase data as a function of frequency is fit to its respective model using effusivity and diffusivity as the fitting parameters. A single fit is all that is required, providing a simple and direct route for determining the film's thermal properties. This routine is greatly preferred over the iterative approach since accurate magnitude data is more difficult to obtain than accurate phase data.

In order to use the fitting routine, a 'clean' set of data is needed. Because an analytical model represents a case were ideal conditions exist, experimental data may vary significantly from values predicted by the analytical model. One contributor to non-ideal conditions within the apparatus of this experiment is the physical thickness of the nichrome heating strip. Contribution due to this condition is thought small, mainly because of nichrome's high thermal conductivity as compared to the surface that it is in contact with. A more pronounced contribution comes from the finite response time of the measurement circuitry. In any case, these effects are minimized by using phase data obtained from measurements of the glass slide's temperature response as a means for producing absolute sample phase data. In doing this, non-ideal conditions are reduced to an acceptable level.

Phase data produced by the measurement system consists of two components. The first component is the actual phase shift at the front surface of the film resulting from application of the periodic heat source. This is the component desired for use in the curve fitting routine. The second is an error component produced by the measurement system. If the fitting routine is carried out with data that still contains the error component, poor thermal characterization of the thin film will result. Phase information obtained from the glass slide is used to remove the erroneous part of the sample data. For instance, if a true phase lag of 21° is present at the surface of the sample with the heat source set at a frequency of 1000 Hz, the measurement system might yield a value of 21.9°. Now, it has been shown that a 45° lag is expected at the surface of the glass slide. However, measurement of the phase shift at 1000 Hz might result in a value of 45.8°. Because the expected value of phase shift is available for the slide, the error produced is also known. For this case, the error is 0.8°. Assuming that an error of the same magnitude is produced by the system for both the slide and the sample, the error calculated using the slide data can be used to offset the sample data. For instance, by subtracting 0.8° from the sample data measured at 1000 Hz, the corrected value becomes 21.1°. The corrected value may not be error free, but is much closer to the actual phase shift at the front surface than prior to correction. The same

correction scheme is used for phase data at each frequency, and the corrected values are used in the curve fitting routine.

The thin film's thermal diffusivity and effusivity result from the fit of phase data to the analytical model for a given temperature. Once these two properties are available, the specific heat is determined with,

$$C_{p1} = \frac{e_1}{\rho_1 \sqrt{\alpha_1}} \tag{3.88}$$

where a density of ρ_1=2220 kg/m^3 is used for the thin film, which corresponds to that of bulk fused silica. The density of a thin film is expected to be lower than that corresponding to bulk material, but in most cases only by a few percent.[21] Therefore, the use of a bulk value is thought to be sufficient for this work. The density is held constant when extracting specific heat at all temperatures. With a value for specific heat, the thermal conductivity is easily calculated with,

$$k_1 = \rho_1 \alpha_1 C_{p1} \tag{3.89}$$

The process is repeated at elevated temperatures with the results from each frequency sweep producing a set of thermal properties for the thin film sample as a function of temperature.

4. EXPERIMENTAL METHOD

Experimental data must be available in order to use the analytical models developed in the previous chapter for purposes of curve fitting. Included in this chapter is a description of the experimental apparatus used for measuring phase shift between heat input and surface temperature of a thin film sample. A procedure for sample preparation is then given. Finally, a method for using the experimental setup with intent on recording phase shift data is presented.

4.1. Apparatus

The experimental configuration used to obtain phase data is centered about a sample emitting infrared radiation in a periodic manner as a result of rapid change in surface temperature. The sample is mounted onto a heater/heat sink configuration capable of providing bulk temperatures in excess of 400°C. The temperature fluctuations are produced on top of this bulk temperature. Fluctuations are generated with resistance heating as a periodic voltage is applied across a thin nichrome strip on the sample's front surface.

The function generator of Fig. 4.1 supplies the periodic voltage across the nichrome strip. Infrared emission from the nichrome strip is captured by a lens, and is focused onto the detection element of an infrared detector. The detector produces an output proportional to the amount of energy striking its surface at any given time. This output is sent on to an amplifier where the signal strength is increased. The signal reaches its final destination at a lock-in amplifier. Here, the signal is compared to that of the function generator's synchronous output, which is in phase with the voltage signal applied across the nichrome heating strip. Internally, the lock-in manipulates both signals and produces values for magnitude and phase shift of the input signal. These values are channeled to a digital display on the front panel of the lock-in for recording.

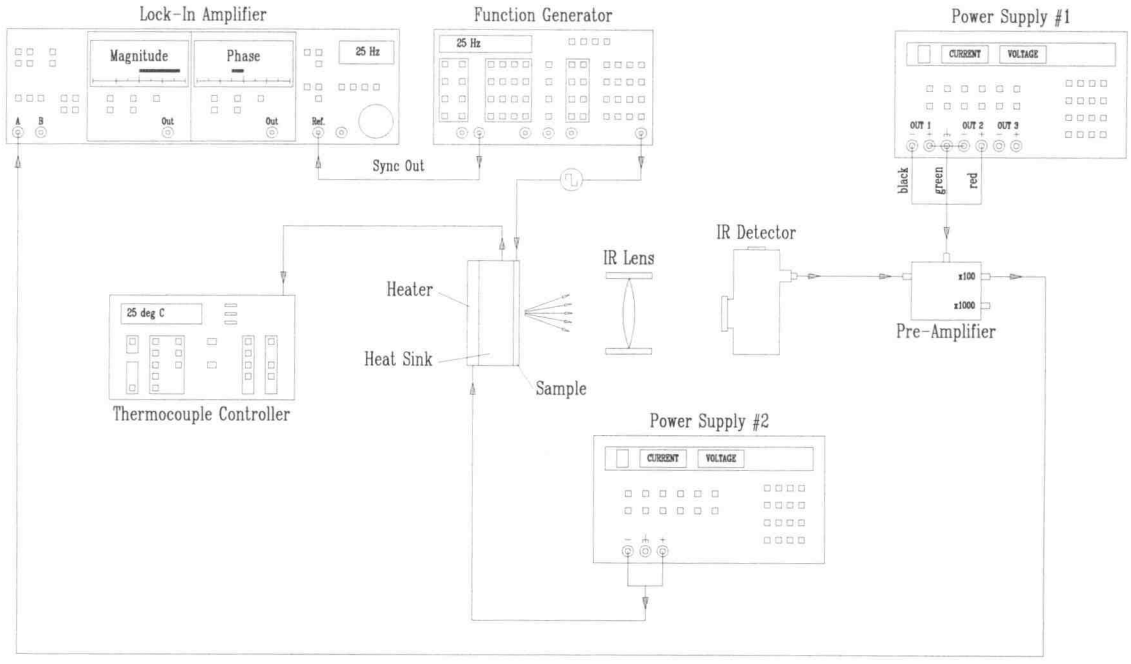

Figure 4.1 Experimental Setup

A description of the physical system is broken into five parts, starting with the sample holder. It should be noted that the term 'sample' as used in this chapter refers to a nichrome/thin film/substrate combination. The term 'sample' is never directed toward the thin film itself, unless otherwise stated. Also, for each data set that is taken for the sample, another is taken for a fused silica slide with an equivalent nichrome layer on its surface. This slide will be referred to as the 'reference standard', or 'standard' from this point forward. The sample and standard are mounted side by side in the sample holder.

4.1.1. Sample Holder

The sample holder consisted of a variety of parts, each providing a useful function in the overall measurement system. For purposes of discussion, this part of the apparatus is broken into the subsystems of macro-adjustment stage, micro-

adjustment stage, heat sink platform, heater/heat sink, and sample with electrical mounting configuration. These subsystems are shown in Fig. 4.2.

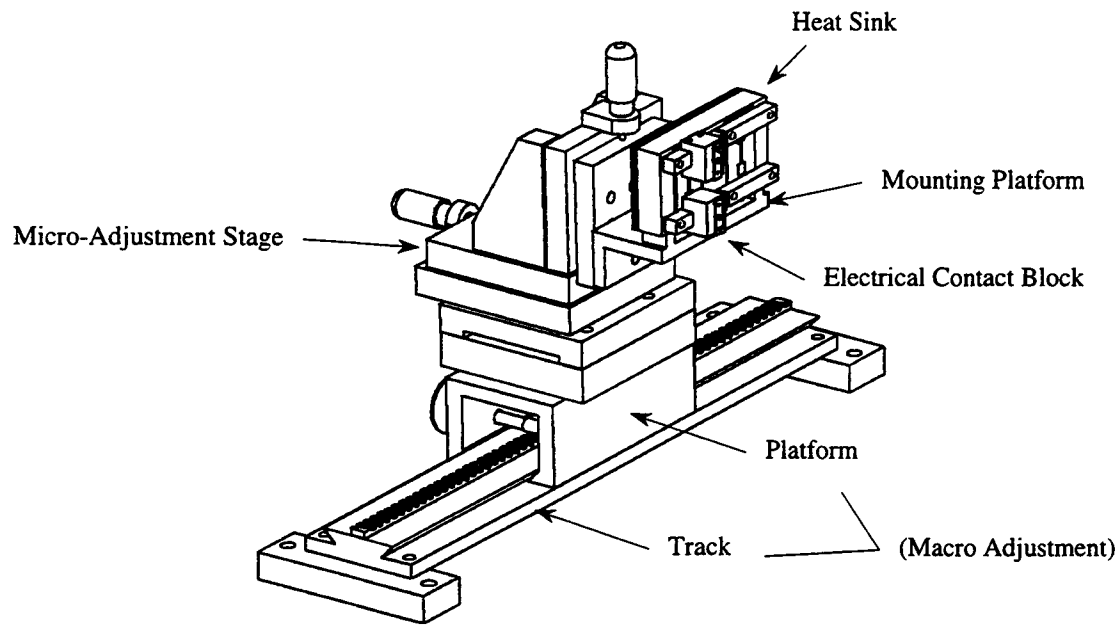

Figure 4.2 Sample Holder

The first subsystem is a macro-adjustment stage. This stage was mounted to an optical table that had $^1/_4$-20 holes spaced on center in 1" (2.54 cm) increments. The stage consisted of a platform/track combination. The track (Edmund Scientific Part# A31,241) was an extruded aluminum piece. Attached lengthwise to the track was a scale graduated in increments of 0.01" and 0.10". The platform (Edmund Scientific Part# A31,240) was capable of up to 10" (25.4 cm) of translation along the track. Motion was provided through a helical rack and pinion by turning an adjustment knob located on the side of the platform. When a desired platform position was reached, the platform was locked into place with a small setscrew. The platform had dimensions of 4"L x $2^1/_4$"W x $1^3/_8$"H (10.16 cm x 5.72 cm x 3.49 cm) and was capable of supporting a maximum load of 15 lbs when mounted horizontally. This adjustment stage was used primarily for shifting between the thin film sample and the fused silica standard.

Mounted directly on top of the macro-adjustment stage was a stainless steel micro-adjustment stage. Where the macro-stage only provided translation along one axis, this stage was capable of providing micro-adjustment in all three dimensions. Possessing this capability was crucial to ensure proper alignment between the emitting surface of the sample, the lens, and the IR detector element. Fine adjustment along each axis of this stage was provided through micrometers. Each micrometer controlled motion along a separate axis and was capable of 0.500" (1.27 cm) translation full scale. Each scale was graduated in units of 0.001". The complete measurement system was designed so that when aligned, each micrometer would read approximately 0.250" (0.635 cm), or half of its full scale value. This allowed for adjustment of each micrometer by 0.250" (0.635 cm) in either direction along its respective axis.

The micro-adjustment stage contained a stainless steel plate at its front surface. On this plate was a pattern of mounting holes, two of which were used to attach a brass platform. The platform was in the shape of an 'L' and was mounted to the stainless steel plate with cylindrical stainless steel spacers as an intermediate layer. Spacers were used in order to increase thermal resistance between the plate and brass platform. Each spacer was $^1/_4$" (0.635 cm) in length and $^3/_8$" (0.953 cm) in diameter. Both spacers also had a wall thickness of approximately 0.025" (0.0635 cm).

A brass heat sink was mounted to the top surface of the brass platform, again with two spacers used to impede heat transfer. These spacers had a $^1/_4$" (0.635 cm) square cross section and a length of approximately 0.3" (0.762 cm). The material used for these spacers was of a ceramic nature. An attempt at using stainless steel spacers was made. However, steel spacers allowed for too much heat flow between the heat sink and mounting platform by conduction. Use of ceramic spacers reduced this heat flow by a large factor, thereby reducing the amount of current required by the resistance heater.

The heat sink was 3"L x $1^1/_2$"W and $^1/_2$" thick (7.62 cm x 3.81 cm x 1.27 cm), which provided an adequate volume for energy storage. Heat was supplied to the sink from a high temperature mica insulated electrical resistance heater (Minco

Part#HM6800-R8.7-L12-T1) rated for temperatures up to 590°C. The heater was mounted to the heat sink in a layered fashion with two stainless steel bolts. The outer layer was a stainless steel backing plate and the middle layer was the mica heater. The plate was used to supply uniform pressure across the heater surface. The manufacturer claimed that without uniform pressure there would be a strong chance of mica layer separation during warm-up. Current was supplied to the resistance heater through a Tektronix Programmable Power Supply (Model# PS2510G).

In order to monitor heat sink temperature, a small hole was drilled into the top surface of the heat sink for placement of a thermocouple. The hole was located lengthwise in the center of the heat sink and approximately $^1/_8$" (0.318 cm) from the sample mounting surface. A thermocouple was inserted into the hole and its leads were routed to a Keithley System Scanning Thermometer (Model# 740) that provided a digital readout of temperature.

The front of the brass heat sink provided a flat surface large enough for side by side placement of the sample and standard (Fig. 4.3). For each, the 'substrate' was placed closest to the heat sink with the nichrome layer facing the detector.

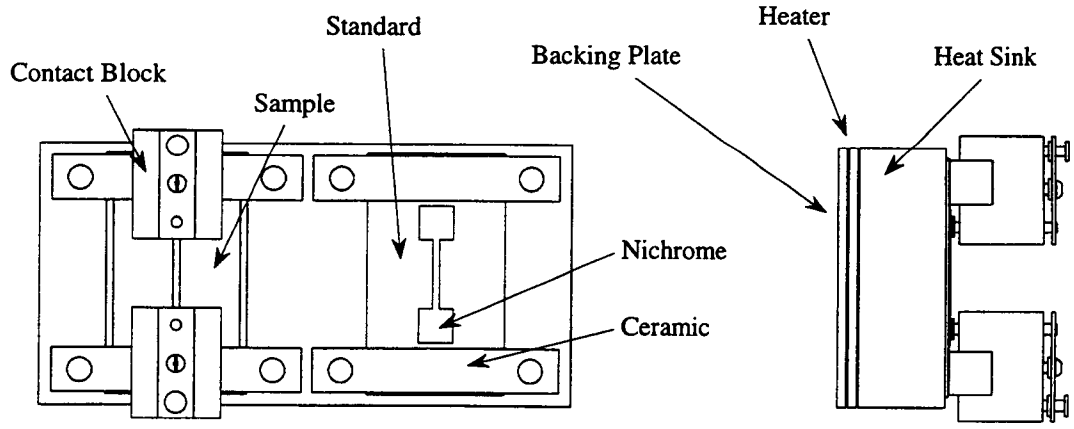

Figure 4.3 Heat Sink Configuration

Both samples were attached independently to the heat sink with stainless steel bolts and machinable ceramic mounting bars. The ceramic bars provided electrical isolation between the heat sink and the contact blocks. Attached to each contact block were opposite leads from a Tektronix Programmable/Arbitrary Function Generator (Model# AFG 5101). The function generator was used to supply a periodic voltage across the leads in the form of a modified square wave. The specific waveform used in the experiment is discussed in the pages to follow.

As evident in the side view of Fig. 4.3, electrical contact between each block and the nichrome contact pad was provided using a basic lever arm principle. The middle 'shaft' of each block was a machine screw with a mating hole that had been threaded into the contact block. As this screw was tightened, pressure was applied to the contact pad through a contact shaft. Likewise, pressure was released by loosening the screw. All components of the contact block were machined from brass. In order to decrease electrical resistance between the brass contact shaft and nichrome contact pad, a soft copper foil (0.001", 2.54×10^{-3} cm) was placed between the two. The foil was folded over three times to provide an effective thickness of approximately 0.003" (7.62×10^{-3} cm) as a gap between the shaft and pad. Using a thickness of 0.003" seemed to protect the thin nichrome contact pad from being heavily scratched at high temperatures as a result of thermal expansion, where a single 0.001" layer did not. Through experimentation it was determined that elevated temperatures produced heavy oxidation on the copper spacers. In later experiments the copper shims were replaced by nickel to reduce this phenomenon.

4.1.2. IR Lens

In order to focus surface emissions emanating from the sample onto the infrared detector's active surface area (1 mm^2), a positive meniscus lens was chosen (Janos Technology Inc. Part# A1200-012). This lens had been fabricated from Zinc Selenide and was specified for transmission of wavelengths ranging from 0.63 μm to

18 μm at a transmission rate of nearly 70%. The lens was $^{3}/_{4}$" (1.905 cm) in diameter and had an effective focal length of 1" (2.54 cm) at its design wavelength (10.6 μm). It was also non-hygroscopic, such that special protection from the atmosphere was not required.

The lens was housed in an Edmund Scientific three-screw adjustable diameter ring mount (Part# P3668) as shown in Fig. 4.4. At the tip of each tightening screw was a protective nylon pad that provided a buffer between the lens and screw. In order to reduce exposure of the lens to sources other than the sample, the lens mount was placed within a lens tube. The lens tube was composed of two pieces. One piece extended toward the sample and the other toward the detector. Each tube was fabricated from aluminum and was painted flat black to minimize internal reflection.

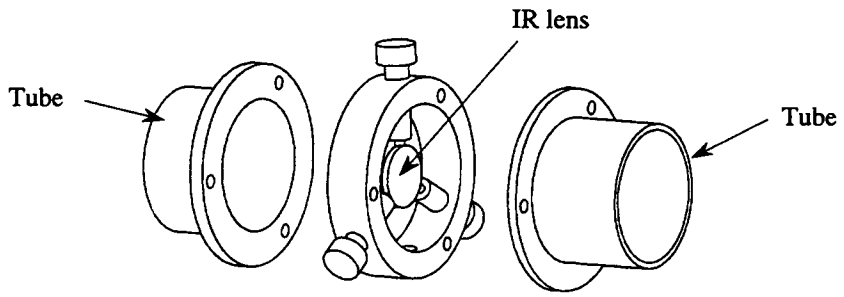

Figure 4.4 Mounted Infrared Lens

The lens mount was fastened to a slotted aluminum bracket by a $^{1}/_{4}$-20 socket head bolt with the bracket sandwiched in-between the bolt and mount (Fig. 4.5). This provided the capability to slide the mount to any location along the 2" x $^{1}/_{4}$" (5.08 cm x 0.635 cm) slot before the bolt was tightened. The slotted bracket was mounted to a miniature three axis positioning stage, which permitted micro-adjustment for aligning components of the focusing system. When the optimal position was reached, each of the three adjustment stages was independently locked into place with a small setscrew.

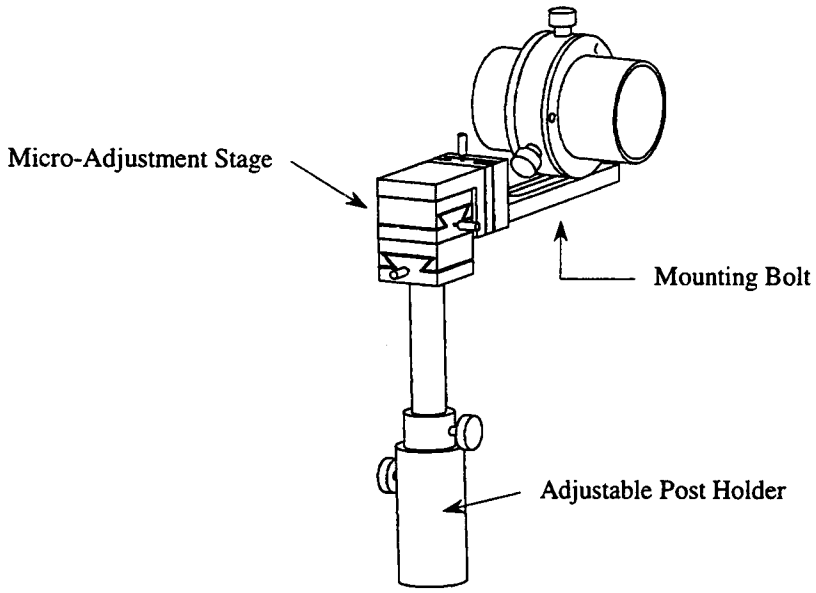

Figure 4.5 Lens Adjustment System

The three axis positioning stage was mounted to a $^1/_2$" (1.27 cm) diameter stainless steel shaft. The shaft had been matched to an adjustable post holder. The post holder provided quick-change capabilities along with the ability to vary lens height. Vertical motion exceeding 1" (2.54 cm) could be achieved with this configuration. The post holder was rigidly fastened to the optical table, placing the lens approximately 2" (5.08 cm) from the surface plane of the samples.

4.1.3. IR Detector

The infrared detector was a very important component of this measurement system. At high heating frequencies (20 kHz) only a small temperature change was expected. Therefore, a sensitive detector with fast response time was required. In order to meet the needs of this system, a Mercury Cadmium Telluride detector (EG&G Judson Part# J15D12-M204-S01M) mounted inside a metal dewar was used (Fig. 4.6).

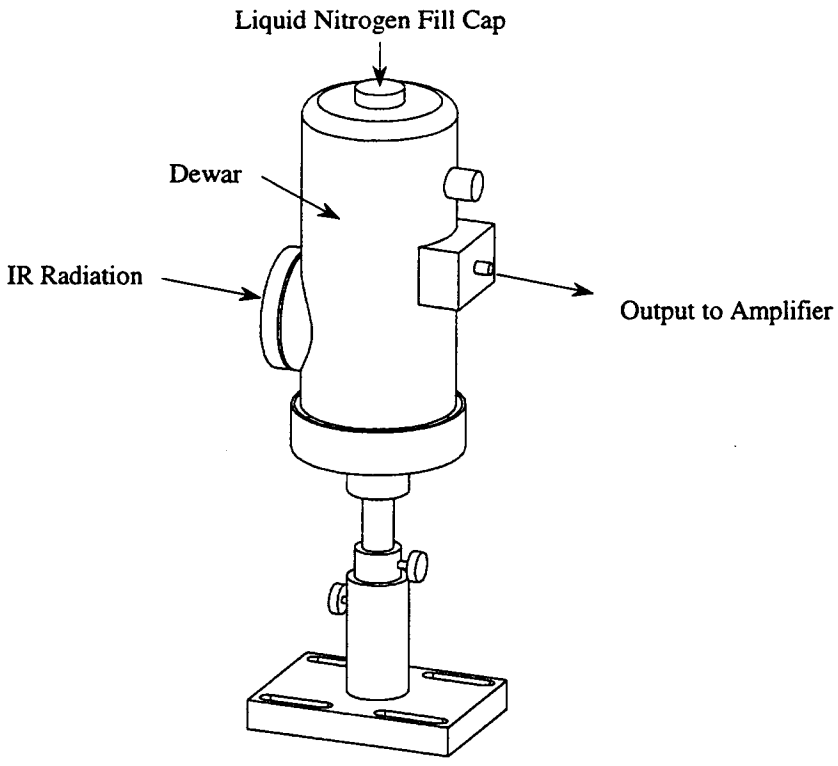

Figure 4.6 Detector/Dewar Combination

This detector operated on the basis of photoconduction where photons with energy greater than that of the detector (HgCdTe) band-gap would excite electrons into the conduction band of the semiconductor. The result was an increase in conductivity of the detector element. In order to sense the change in conductivity, a bias current was applied through the detector element. This current was provided through the amplifier circuitry discussed in the following section.

The detector was designed to operate cryogenically at 77 K and would be responsive to radiation at wavelengths between 2 μm and 12 μm, with optimum performance achieved in the 8-12 μm range if used according to the manufacturer's specifications. In order to maintain the 77 K operating temperature that was specified by the manufacturer, the dewar was filled with liquid nitrogen. The dewar hold time was rated at approximately 10 hours.

The base of the detector was mounted to a cylindrical platform, permitting rotation for purposes of squaring the detection plane with the focal axis of the lens. The platform was connected to an adjustable post holder, which functioned as a quick release holder and provided the capability of linear motion for detector height adjustment. The postholder was mounted directly to a stainless steel spacer. Machined within this spacer were 1" (2.54 cm) long slots with spacing that matched the optical table hole pattern. The spacer was mounted to the optical table through these slots to allow for adjustment of the detector along the focusing axis of the lens.

A scaled representation of the apparatus is given in Figs. 4.7 and 4.8. The figures illustrate the relative spacing used to position the various components of the system. Note that the optical table had an evenly spaced pattern of holes that were 1" (2.54 cm) apart. If desired, approximate component dimensions and spacing can be obtained from the figures by using the optical table hole pattern as a scaling reference.

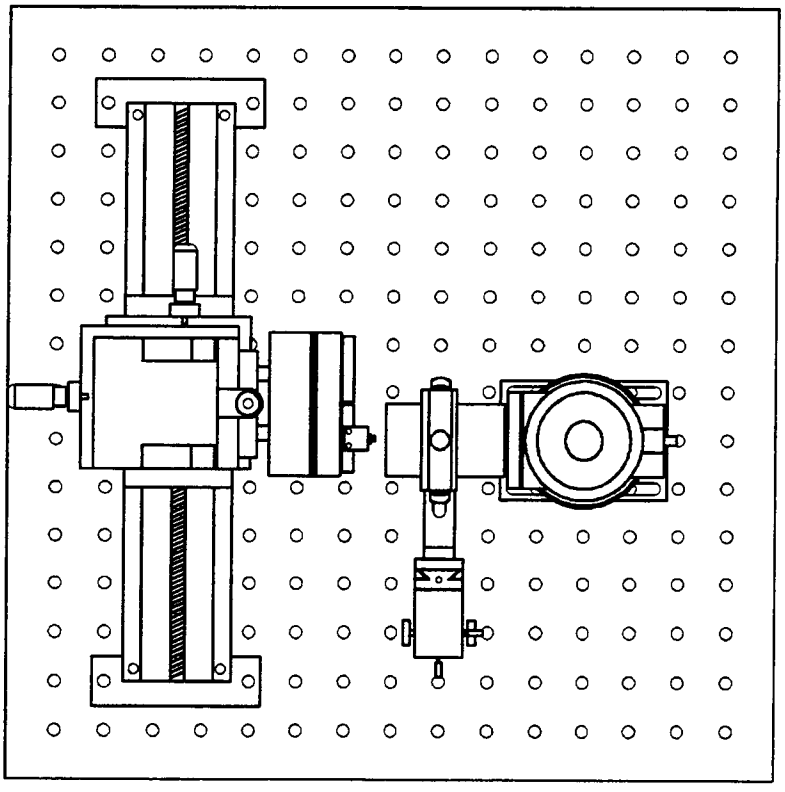

Figure 4.7 Top View: Scaled Representation of System Components

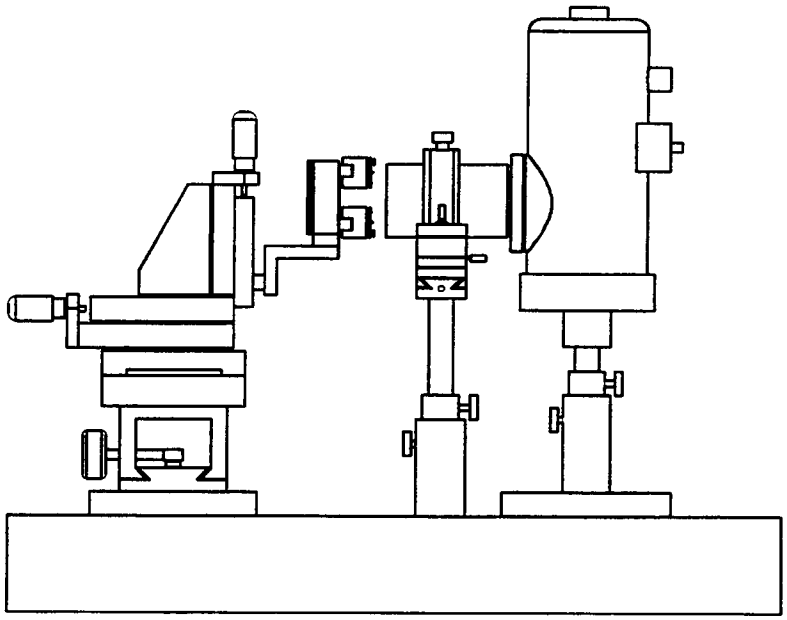

Figure 4.8 Front View: Scaled Representation of System Components

4.1.4. Pre Amplifier

As stated earlier, a constant bias current had to be supplied through the element of the photoconductive detector in order to sense a change in the element's resistance. With constant current, a change in resistance would be accompanied by a change in voltage across the element. In this system, the voltage change was composed of a DC component provided by the bulk temperature of the sample and an AC component from the temperature fluctuations. Of real interest was the signal that resulted only from surface fluctuations of the sample. Therefore, an AC pre-amplifier was desired that effectively blocked any DC voltage components produced at the detector output.

Since the detector of this system was a low impedance device, a low noise pre-amplifier was required to amplify the signal for the lock-in. An EG&G Judson PA-101 voltage mode pre-amplifier was used for this purpose. When ordered together, EG&G Judson could match the PA-101 bias circuitry (resistor) to the resistance of the

infrared detector, producing a pair that ensured an optimum bias current through the detector element.

The pre-amplifier was powered by a Tektronix PS2521 Programmable Power Supply. Prior to choosing the power supply, a battery pack was used to power the amplifier for stable operation. However, battery drain produced undesirable drift in the measurement system and the pack was discarded. The power supply was configured for bipolar operation at ±15 V. Three leads were furnished with the amplifier for connection to the power supply (black, green, and red). The black lead was connected to the negative terminal of output one on the power supply, the green lead was connected to ground, and the red lead was connected to the positive terminal of output two (Fig. 4.1). The pre-amplifier bias resistance of this system was 402 Ω. This resistance, along with +15 V supplied by the power supply, produced a bias current of 31.2 mA in the detector element.

The PA-101 voltage pre-amplifier had two output stages. The first stage produced an inverted signal at amplification of 100X. This stage had a bandwidth of 10 Hz - 1 MHz. The second was a 10X stage in series with the first. Thus, its output was no longer inverted. This stage produced an effective overall gain of 1000X, but bandwidth would be reduced to 10 Hz - 200 kHz. Only stage one of the amplifier was used during this experiment.

4.1.5. Lock In Amplifier

In simple terms, Fourier's theorem states that any signal can be represented by the sum of many sine waves, each with a carefully related frequency, amplitude, and phase. When a very small AC signal is embedded within a large amount of noise, a lock-in amplifier can be used to accurately single out Fourier components of that signal. Component acquisition is accomplished using a technique known as phase sensitive detection where a single Fourier component is extracted from the signal at a predetermined frequency, and all other signal components (including noise) are filtered

out. The predetermined frequency is provided by a reference signal. The reference signal must be of the same frequency as the signal being measured, and its phase must not change with time. If the frequencies are equal, the component extracted by the lock-in will commonly be the first harmonic of the input signal.

A basic analog lock-in usually provides phase and amplitude of the first harmonic of the input signal only, where phase is measured with respect to the reference signal. Most modern digital lock-in amplifiers provide access to multiple harmonics, allowing complete signal reconstruction if desired. In this apparatus, a digital lock-in amplifier was used with intent placed on accurate measurement of the first harmonic only and not on signal reconstruction. A Stanford Research Systems Model# SR830 DSP (Digital Signal Processing) dual channel lock-in amplifier was used for this system component. This lock-in amplifier also allows simultaneous display of both phase and magnitude of the specified harmonic, which makes data recording convenient. The measured phase shift was given in degrees and amplitude was in RMS volts.

As a simple example, say that the input to the lock-in is supplied by a function generator in the form of a square wave with a 1 V amplitude and frequency $\omega=2\pi f$. Also, the reference signal is supplied by the function generator's synchronous output, which is at the same frequency and phase as the input signal. This square wave could be expressed with,

$$S(t) = 1.273\sin(\omega t) + 0.4244\sin(3\omega t) + 0.2546\sin(5\omega t) + \ldots\ldots \qquad (4.1)$$

With the lock-in amplifier set to measure the first harmonic of the input signal, the first sine component in the above series would be detected. However, a 1.273 V amplitude would not be displayed on the lock-in's front panel. Instead, the lock-in would display the signal's RMS value, or $1.273\,\mathrm{V}/\sqrt{2} = 0.90\,\mathrm{V}$. Also displayed would be a phase shift of zero, as expected. Now, knowledge of the second harmonic could be provided by a single push of a button. However, detection of the second harmonic for this case would yield an amplitude and phase shift of zero. Likewise, the

third harmonic would produce an amplitude reading of 0.30 V, also shifted zero degrees in phase.

The experiment was set up in a manner similar to the example above. A function generator was used to supply a periodic voltage in the form of a modified square wave across the specimen and the function generator's synchronous output was used as the reference signal. The square wave was modified to produce a situation where the periodic heating signal at the sample's front surface was in phase with the reference signal of the lock-in amplifier. This was accomplished by using a voltage whose DC value was offset to produce a signal varying between zero and twice its amplitude. The synchronous signal was observed on an oscilloscope to be approximately 3.5 V p-p.

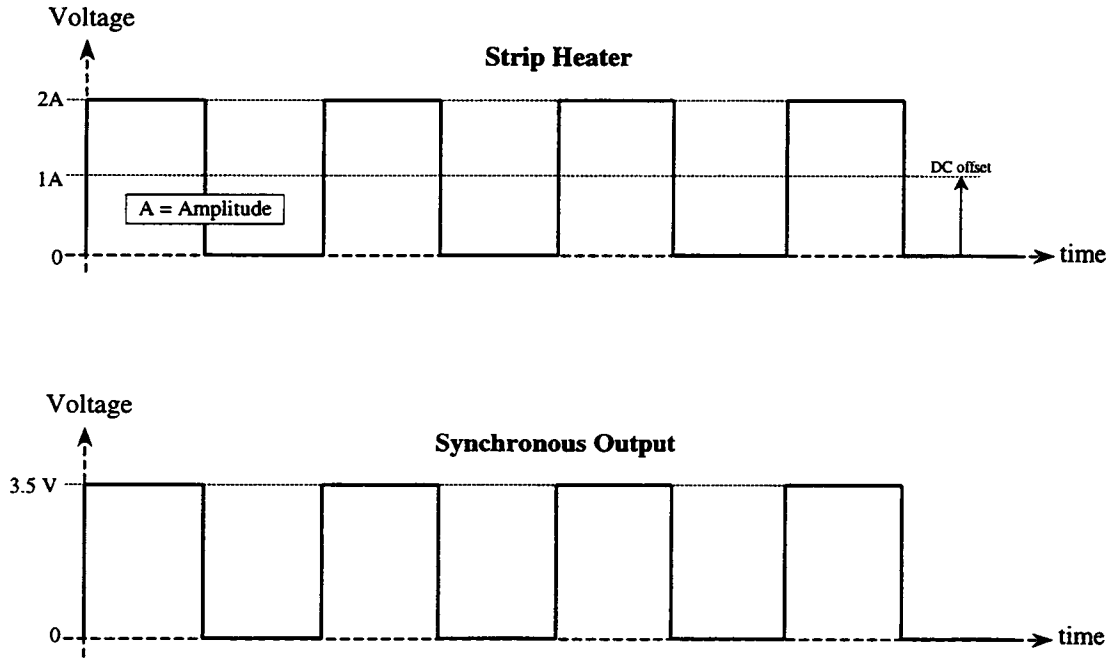

Figure 4.9 Voltage Signals

4.2. Specimen Preparation

For each trial of an experiment, both a sample and a standard were required. The sample was a three layered structure and consisted of a silicon substrate, an oxide layer (SiO_2), and a nichrome heating strip. The standard was a two layered structure composed of a fused silica slide and a nichrome heating strip. The method used to fabricate both a sample and standard is presented in this section.

Each sample started out as a section of 675 μm thick silicon wafer that was 6" (15.24 cm) in diameter. The silicon wafer was placed in a heated, oxygen rich environment and a 1.72 μm oxide layer was allowed to form. This oxide layer was the thin film to be studied. The wafer was then sliced into rectangular pieces with dimensions of 3.5 cm x 2.0 cm (1.378" x 0.787").

The standards were produced from an oversized fused silica laboratory slide. Each slide was 1 mm (0.0394") thick. The slide was first marked at 3.5 cm x 2.0 cm (1.378" x 0.787") and then cut to size. Because fused silica is a very hard material, cutting could not be accomplished by 'ordinary' means. Instead, a slow and tedious process of abrasive cutting was carried out with a stainless steel wire used as the cutting tool. A total of five pieces were produced using this process.

A nichrome layer (80% Nickel / 20% Chromium) was deposited on each of the specimens using an e-beam evaporation process. Deposition was completed in pairs, where a layer of nichrome was concurrently placed on one thin film sample and one piece of fused silica. To do this, a mask with two patterns of equal dimensions was machined out of a thin piece of aluminum. On top of one pattern was placed a sample, and on the other a fused silica standard. The mask was then situated on top of a support stand within the deposition vacuum system and the evaporation process was initiated. Nichrome thickness was monitored continuously with a crystal oscillator as the deposition process was carried out. Two specimens of equal heating strip thickness were made available each time this process was carried out.

The deposition process was completed a total of four times, producing four specimen pairs. However, not all pairs were alike. Two dimensions were varied

between deposition processes. These variables were heating strip thickness and strip width. The thickness was a function of evaporation tank hold time and deposition rate, and the strip width was a function of the mask dimensions only. In varying these parameters, the specimen pairs shown in Table 4.1 were produced. The starred specimen pair (C^*) had an additional 50 nm layer of nickel deposited on top of its nichrome contact pads.

Table 4.1 Dimensional Variation of Nichrome Heating Strips

Specimen Pair	thickness (nm)	width (mm)	resistance (Ω)
A	100	1	160
B	50	1	300
C	50	2	110
C^*	50	2	150

A visual examination was performed on each specimen pair after the nichrome depositions were complete. By holding the standard of each specimen pair up to a source of white light, it was found that the 100 nm (A) heating strip was essentially opaque to the light and allowed transmission of less than 5%. On the other hand, each 50 nm strip allowed a larger portion (20% - 40%) of the light to pass through its thickness. In any case, the deposition process produced an excellent bond at the nichrome/specimen interface for all samples produced by the process as well as for each of the standards. All interfacial bonds were strong enough so that the nichrome could not be smeared off with a simple swipe of a cloth or finger, but required heavy scratching in order to degrade the heating strip.

All of the other dimensions, such as contact pad width and strip height were not changed between the deposition process of each specimen pair. The dimensions of the nichrome strips are shown in Fig. 4.10 along with a relative view of a 2 mm (0.0787") wide strip as compared to a 1 mm (0.0394") wide strip. It is not specifically

shown in the figure, but each nichrome strip was centered in both directions on the medium that it was deposited.

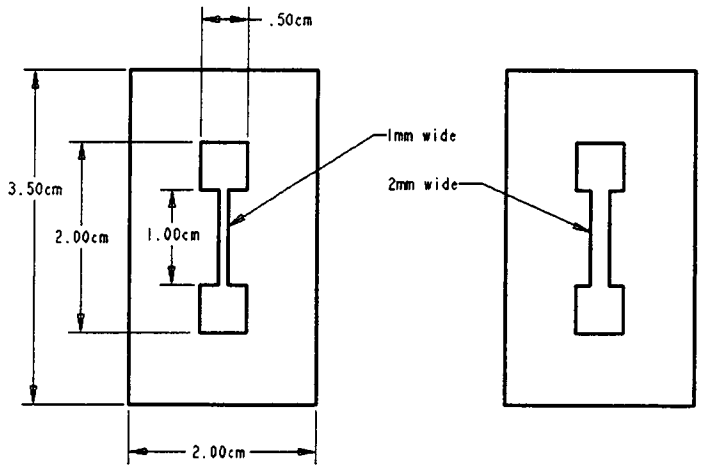

Figure 4.10 Dimensions of Nichrome Heating Strip

4.3. Experimental Technique

Recording of experimental data for determination of thin film properties was very straightforward for this process provided that the experimental apparatus had already been properly aligned. Basically, a specimen pair was placed in the sample holder and was heated to a temperature at which thermal properties were desired. Then, with the detector focused on the sample, phase data was recorded though a range of heating frequencies. When the frequency sweep was complete, the apparatus was adjusted to place the standard in the detector's line of sight. Phase was again measured at the same frequencies. The frequency dependent phase information obtained with the experimental apparatus was then used to extract the thin film thermal properties from. This section presents a detailed description on all steps taken during the process mentioned above, beginning with a brief discussion on how initial alignment between the specimen, lens, and detector was accomplished.

4.3.1. Initial Alignment

Prior to phase measurements, it was imperative that the focal system was properly aligned. This was achieved in two steps. The first step resulted in axial alignment between the detector, lens, and center of the heat sink. This was performed without a specimen pair in the sample holder. The second step brought the front surface of a specimen into focus on the detector element. This step will be discussed as though a specimen pair had already been mounted in the sample holder and the system was up and running, even though specimen installation and system settings are not covered until the following sections of this chapter.

To attain axial alignment, a 1 mm (0.0394") thick glass slide was first fastened in the sample holder. Then a piece of white tape was placed on the front surface of the slide. Placed directly on top of the white tape was a piece of black tape from which a small hole had been cut. The black piece was placed such that the hole was centered with respect to the heat sink's height. The hole was approximately 1 mm (0.0394") in diameter. This provided a small white circle within a black 'background'.

Next, the white circle was illuminated with a very small red dot using a Helium-Neon laser. The black tape helped minimize reflection of stray laser radiation. As all lights were turned off in the room, a blurred red image appeared on the detector window resulting from transmission of the slide image through the lens. The lens and detector position were carefully adjusted until the red image came into focus (red dot) at the center of the detector window. The result of this step was axial alignment of the focal system.

The detector element was located approximately 8 mm (0.315") behind the detector window. This led to the misconception that moving the detector 8 mm closer to the lens would result in complete focus of the system. However, it was realized that the index of refraction of the Zinc Selenide lens was wavelength dependent, and thus was the focal length. Helium Neon laser emission was near 0.7 μm, where specimen emission was closer to 10 μm. Therefore, while a simple 8 mm movement of the detector may have brought the laser light into focus on the detector element, it would

not have produced the same effect on infrared emission from the surface of a specimen.

In order to bring the desired focal point onto the detector element, infrared radiation from the specimen surface was required. To achieve this, a specimen was mounted in the sample holder and a periodic voltage was applied across the nichrome heating strip. Then, transverse position of the nichrome strip was varied along with axial distance between the detector and lens. With each modification, signal magnitude was carefully observed at the lock-in amplifier. The system was said to be in focus at the detector position that produced maximum signal magnitude as measured by the lock-in.

Alignment was now complete, but only for the current specimen. However, the complete alignment scheme did not have to be repeated every time measurement of a new specimen was desired. As long as the detector and lens holder position remained unchanged, emission could be brought into focus by varying only transverse location of the nichrome strip until a point of maximum signal was achieved. For instance, if recording of sample data was complete, the standard was brought into the detector's line of sight using the sample holder's rack and pinion knob. Then, the nichrome position was fine-tuned with the micro-adjustment stage until a point of maximum signal was achieved. Surface emission was now in focus on the detector element.

4.3.2. Specimen Installation

In order to place a specimen pair into the sample holder, the heat sink first had to be dismounted from the brass platform. The sink was then placed on a flat table with its front surface facing up. Next, the screw that places pressure between the contact rod and the nichrome pad was gently loosened for each block. Each screw that fastened the ceramic mounting bars to the heat sink was extracted, and the ceramic bars (with contact block still attached) were removed from the surface. The bars were

separated so that each could be placed in its original location upon reassembly. This removed one point of possible inconsistency between specimen runs. The current specimen pair was now free for removal, and was placed in a safe location for use at a later time.

The heat sink surface was ready for placement of a new specimen pair. First, the standard was placed on one side of the sink and was centered with respect to sink height. Next, the ceramic mounting bars were carefully placed on the standard's surface. Then each mounting bolt was hand tightened, making sure that an even pressure was applied between surfaces of the bars and the standard. If all mating surfaces appeared to be flat with respect to each other after hand tightening the ceramic mounting bolts, the bolts were secured using an Allen wrench. Then, two strips were cut from a piece of 0.001" (0.0254 mm) copper foil, each strip 5 mm x 15 mm (0.197" x 0.591") in size. The strips were folded three times lengthwise to produce a 5 mm (0.197") square piece of copper with a thickness of 0.003" (0.0762 mm). The copper shims were placed directly onto the nichrome contact pads and the contact rods were lowered, thus completing the installation process for the standard.

A similar process was used to fasten the sample to the heat sink. However, the substrate was not placed in direct contact with the heat sink. Instead, a fused silica slide of the same dimensions as the sample was placed between the two. Because the silicon substrate was a semiconductor, problems due to capacitive coupling between the heat sink and the nichrome heating strip were produced when the silicon was placed in direct contact with the brass heat sink. The fused silica slide was used to eliminate undesirable effects due to electrical coupling as current passed through the nichrome strip. With the specimen pair set in place, the heat sink was set back onto the ceramic insulation blocks and was secured to the brass mounting platform.

Great care was required during specimen installation. If a threaded element was synched too tight, damage to a number of components was possible. Application of excess pressure on a sample/standard supplied by a ceramic mounting bar was likely to break either the bar or the sample/standard. It was also possible to crack a ceramic mounting bar by over tightening a block's setscrews during assembly of the contact

block and bar. Finally, care had to be taken when lowering the contact rod down onto the nichrome pad. Excessive pressure produced undesirable scratching of the thin nichrome strip, causing great difficulty in obtaining adequate electrical contact. Although the copper cushions reduced scratching, they did not prevent it.

4.3.3. System Initialization

Each time the apparatus was used, the measurement system had to first be "warmed up". This not only included bringing the specimen pair up to temperature, but also making sure that the detector had reached a state of thermal equilibrium and that all electrical components were settled.

Starting up the measurement system began with filling the detector dewar with liquid nitrogen. A funnel that was supplied with the dewar was first inserted into the dewar and a small amount of nitrogen was poured in. Because components inside the dewar were at room temperature prior to filling, rapid nitrogen boil-off occurred during initial pours. The nitrogen in the dewar was allowed to settle for 10-15 seconds before any more was added. This was repeated until the dewar was full, as evident by the discharge of small liquid nitrogen "bubbles" from the funnel insertion point on the dewar's top surface. Once the detector was full of liquid nitrogen, the power supply that fed the pre-amplifier was turned on and both outputs were set to 15 V. It should be noted that enabling outputs of this power supply without proper connection between the pre-amp and a 'cooled detector' is potentially harmful to the system.

Next, the function generator output leads were connected across the nichrome strip. The leads were attached directly to the contact blocks by alligator clips. The black lead was connected to the upper block and the red to the lower. Then the function generator was turned on and set for square wave operation with the signal amplitude equal to 4.98 V and an offset of 2.49 V. This produced an output ranging from zero volts to 9.96 V (the function generator does not use the standard definition of 'offset'). However, the voltage across the strip was lower than 9.96 V due to

loading of the function generator by the strip resistance. This resistance varied between 100 Ω - 300 Ω depending on strip width and thickness. With the voltage and offset as defined, heating was either on or off and was very similar to that produced by a heat lamp and chopping wheel configuration. Figure 4.11 shows the temperature response of a fused silica standard that was exposed to three different heating frequencies. The plots were generated with the standard of specimen pair C^* at room temperature (R=150 Ω).

In disagreement with the scale below each individual oscilloscope plot, the vertical distance spanning a single square represents 5 V for the periodic heating signal and 5 mV for the temperature signal. The scale below each plot was generated with the scope set for signal amplification at 10X. As mentioned previously, the first amplification stage of the pre-amplifier produces an inverted signal. Therefore, in order to properly display the temperature response (with respect to the heating signal), the signal of Channel 2 had to be inverted. This was accomplished by utilizing the invert option of the scope. During recording of experimental data the signal inversion was easily accounted for by using a dial to 'offset' the phase displayed on the lock-in's front panel by 180°. A digital lock-in provides this option, which proved useful for recording data. The loading of the function generator by the strip resistance is clearly visible in the heating signal of each plot.

The heating signal was set to 9.96 V p-p at the function generator, but the actual signal picked up by the scope was less than 8 V p-p. Figure 4.11 also shows that the amplitude of the temperature response decreased with an increase in frequency, thus verifying the result predicted by Eq. (3.27) of the first analytical model. The infrared detector and pre-amplifier produced a signal that was approximately 6 mV p-p at 500 Hz, which decreased to a value near 1 mV p-p at a heating frequency of 5000 Hz. A lag, which remained constant with frequency, was also evident in the temperature response with respect to the heating signal. The analytical model had also predicted that phase would be constant.

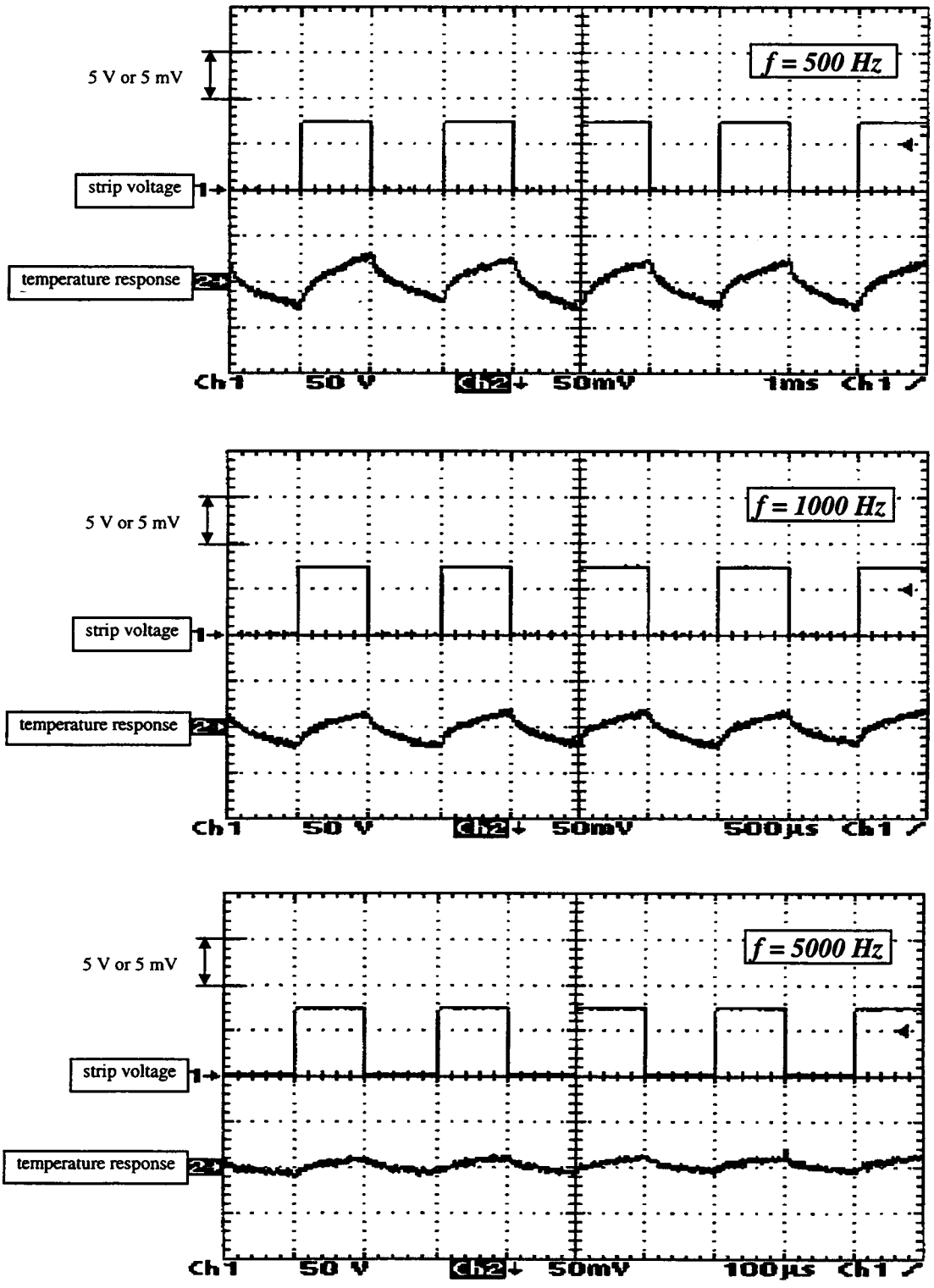

Figure 4.11 Temperature Response to Square Wave Heating Signal

The next step during system initialization was to switch on the lock-in amplifier. The lock-in provided a front panel where numerous operating characteristics could be changed through push-buttons and dials. The initial lock-in settings are summarized in Table 4.2 below.

Table 4.2 Lock-In Amplifier Settings

Time Constant	3sec	Reserve	normal
Time Constant	18dB	Notch Filters	off
Sensitivity	(varies)	CH1 Output	R (magnitude)
Synchronous Filter	off	CH2 Output	θ (phase)
Signal Input	A	Trigger	positive edge
Coupling	AC	Phase	+180°
Ground	float	Harmonic	1^{st}

All of these settings remained unchanged during any given frequency sweep except sensitivity. The sensitivity setting varied with input signal strength, and thus with frequency. Sensitivity was adjusted with frequency to keep the lock-in amplifier away from an undesirable mode of operation where possibility of overloading existed.

Finally, the mica resistance heater was started by turning its power supply on. With the power supply output enabled, DC voltage was varied until the desired heat sink temperature was achieved. Because of fused silica's low thermal conductivity and possibly an interface resistance between a specimen and the heat sink, the temperature at the front surface of a specimen was found to be less than the heat sink temperature as read at the thermocouple controller. Figure 4.12 was generated with experimental data to provide an approximate means of correcting the temperature difference encountered.

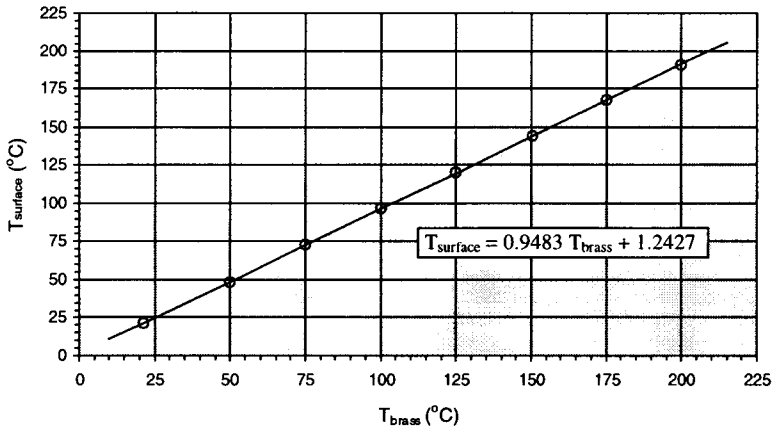

Figure 4.12 Surface Temperature Correction

Surface temperature data was obtained by attaching the bead of a small thermocouple to the front surface of a blank sample (no nichrome) using a highly conductive epoxy. This sample was then mounted into the sample holder with a fused silica slide placed between the heat sink and silicon substrate, mimicking the configuration used in an experimental run. The thermocouple leads were then wired to the thermocouple controller and the resistance heater was started. The heat sink was taken up to temperatures of 50, 75, 100, 125, 150, 175, and 200°C respectively. While at each sink temperature, corresponding surface temperature data was recorded. Finally, surface temperature was plotted against heat sink temperature, and linear regression was used to determine an equation of the best fit line between the data points. It should be noted that the correction curve was used as a way to 'back calculate' surface temperature for specimen pair A. For instance, results are given for a surface temperature of 190.0°C but data was taken for a heat sink temperature of 200°C. On the other hand, surface temperature for all other specimen pairs has been 'forward calculated', where heat sink temperature was pre-determined in order to produce a desired surface temperature. As an example, a surface temperature of 300°C resulted from taking the heat sink up to 315°C.

4.3.4. Frequency Sweep

The system was allowed to "warm up" as explained in the previous section for approximately one hour prior to initial measurements. When the system had reached a state of equilibrium, the measurement process began by recording phase shift with the heating frequency set to 500 Hz. Next, the frequency was set to 1000 Hz and phase shift was recorded. Phase was again recorded at 2000 Hz. This process was carried through until phase at 20 kHz had been measured. To ensure that the detector was operating at or near its optimum temperature for the entire range of measurement frequencies, the dewar was 'topped off' with liquid nitrogen after every fourth or fifth measurement.

When a complete set of phase data was available for the current specimen, say the thin film sample, then the sample holder was shifted to place the reference in front of the detector. The function generator leads were transferred to the new specimen's contact blocks and the frequency was set to 25 Hz. The system was allowed to sit in this state for five to ten minutes, permitting a sufficient time for the system to reach a pseudo steady state condition. The frequency sweep was then repeated by recording phase data at the same frequencies used for the previous specimen, again starting at 500 Hz.

After this sweep was complete, the heat sink temperature was increased to the next value where thermal properties were of interest. When thermal equilibrium existed within the system, the phase measurement process was repeated. The sample holder was kept in place so that the first sweep could be carried out on the current specimen. Translation between sample and standard occurred after this sweep was complete. As an example, say that the system was initialized to produce a surface temperature of 100°C with the sample in front of the detector. Phase data would first be taken for the sample at this temperature. Then data for the standard would be recorded. Next, the heat sink temperature would be increased to produce a surface temperature of 150°C. Now, a frequency sweep would be carried out with the standard still placed in front of the detector, followed by a sweep with the sample.

This reduced measurement time by removing an adjustment step between temperature runs.

In order to keep thermal cycling to a minimum, phase data was taken at as many temperatures that a single sitting would allow. For instance, it was more desirable to take consecutive measurements at 200°C, 250°C, and 300°C without shutting the system down as compared with measuring only one temperature per day for three consecutive days. Thermal cycling produced undesirable effects such as scratching of the nichrome contact pads, which was possibly due to expansion of the contact bar. Detrimental temperature effects were also notable above 200°C with the formation of an oxide layer on the nichrome heating strip. Heavy oxidation also occurred on the copper shims at high temperatures. These oxide layers prevented electrical contact between the brass contact bars and the nichrome. In order to reduce the effects of oxidation, the use of nickel shims was examined. Also, a thin layer of nickel deposited on top of the nichrome contact pads (specimen pair C^*) was looked at. Although each of these solutions was only studied briefly, the pair together produced promising results.

5. RESULTS & DISCUSSION

The results for each specimen pair of Table 4.1 are presented in this chapter. Specimen pair A was studied extensively, but exclusively at room temperature during original trials of the experiment. Therefore, only the results obtained using the final experimental configuration are presented for this pair. Specimen pairs B and C are presented with results obtained at temperatures ranging from 25°C to 300°C. Finally, results for specimen pair C^* are given. This specimen was not studied as a means for calculating thermal properties. However, its results provide useful insight into possibilities for decreasing oxide formation on the surface of the nichrome heating strips at elevated temperatures.

5.1. Specimen Pair A : 1 mm x 100 nm

During initial trials of the experiment, specimen pair A was used extensively to overcome many obstacles that were not obvious at the onset of this project. For instance, providing proper electrical isolation between the sample and the heat sink was an obstacle that needed to be conquered. This was ultimately accomplished by placing the fused silica slide between the sample and heat sink as explained in the previous chapter. However, this seemingly simple solution did not come without an effort involving a great deal of trial and error. In any case, specimen pair A was used primarily to eliminate undesirable 'bugs' from the measurement system.

With the system finally operating near an optimal configuration, phase data was recorded at room temperature for specimen pair A. A set of corrected data (using the standard) is plotted against frequency in Fig. 5.1. The experimental data points obtained using the measurement system are represented in the figure with open circles and the continuous line passing 'through' the data points resulted from a two parameter fit of the data to the analytical model. The thin film's diffusivity (α_1) and

effusivity (e_1) were used as the parameters in the fitting routine. The curve fit was carried out twice for this set of data. Each fit utilized a different thermal conductivity of silicon (k_2), and thus a different effusivity (e_2). Both fits resulted in identical values for phase shift at any given frequency regardless of the thermal conductivity chosen for the silicon substrate. Each fit also produced equivalent values for thermal diffusivity of the thin film, thereby showing the strong dependence that front surface phase data has on this property. However, the film's effusivity did change as the silicon thermal conductivity was altered. The values used in the fitting routine for thermal conductivity and effusivity of silicon are shown directly on the figure along with the film properties (fitting parameters) that resulted from each fit. The calculated values of thin film thermal conductivity and specific heat are presented in Table 5.1 toward the end of the chapter, along with values obtained from use of the other specimen pairs.

Figure 5.1 shows that the phase data obtained with this specimen pair followed the general trend that was predicted by the mathematical model. However, a closer relationship between the two was desired, specifically at the low frequency data point (500 Hz). The effect that the finite nichrome thickness had on the experimental data was studied as a first step toward achieving this goal. Specimen pair B was produced solely for this purpose, whose results are presented in the following section.

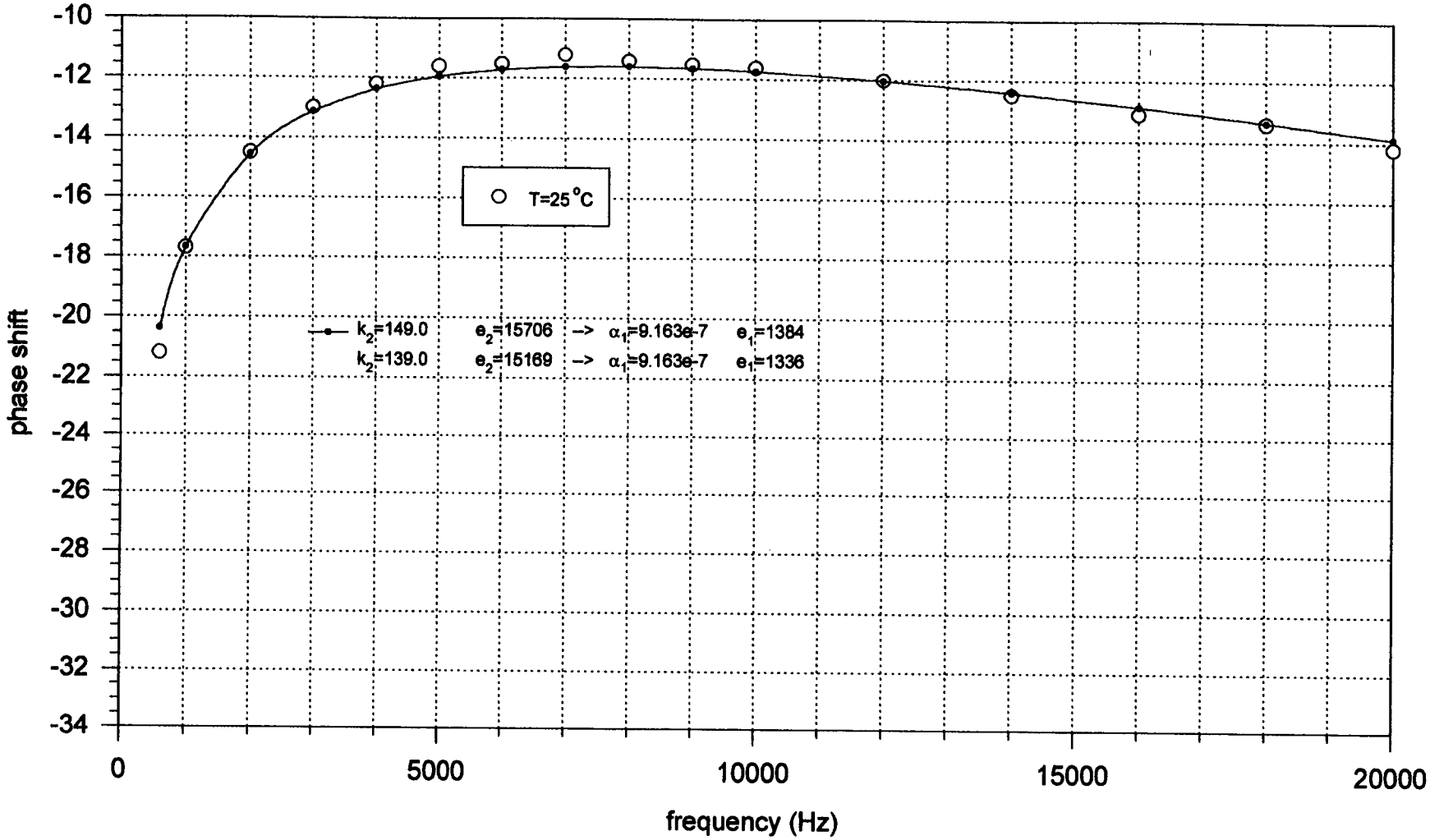

Figure 5.1 Curve Fit Results: Specimen Pair A

5.2. Specimen Pair B : 1 mm x 50 nm

As evident by the curve fit for the specimen pair with 100 nm thick nichrome heating strips, the corrected phase data was not well represented by the analytical model, especially at the low frequency test point of 500 Hz. A specimen pair with a strip thickness of 50 nm was analyzed in order to determine if the finite thickness of the nichrome was a significant factor within the measurement system.

A comparison between the two thickness values was made on all of the raw phase data obtained at room temperature for specimen pairs A and B. Figure 5.2 shows that the strip thickness did affect the phase data obtained by the measurement system. More importantly, the data strayed from the values predicted by the analytical model by a larger amount for the specimen pair with 100 nm strips (A) than for the pair with 50 nm strips (B). This was most apparent for the data points corresponding to each SiO_2 standard. Even though the corrected values were approximately equal for both pairs, a significant difference was still observed at the lower frequencies.

In order to provide an idea of the signal strength detected by the lock-in amplifier, a comparison of magnitude data for specimen pairs A and B is presented in Fig. 5.3. The upper half of the figure represents data taken for each thin film sample and the lower portion represents data obtained with the fused silica standards. All data presented in the figure corresponds to a temperature of 25°C. Figure 5.3 shows that the sample and standard of specimen pair A both produced a signal of larger magnitude as compared to that found with the sample and standard of specimen pair B. The electrical resistance of each nichrome heating strip of pair A was approximately 160 Ω. With the function generator voltage set for operation as discussed in the previous chapter (9.96 V p-p), the RMS voltage across the leads was measured to be 3.9 V for each strip of this pair, which led to a current of 24 mA passing through the strips. Thus, it is estimated that 90 mW of power was dissipated as a result of I^2R heating, or an equivalent heat flux of 0.9 W/cm^2 across a heating strip that is 1 mm wide and 1 cm long. On the other hand, the resistance of the heating strips of pair B was approximately 300 Ω. Because of the larger resistance, a smaller current was

required through the strips in order to maintain the same voltage across the leads as produced for specimen pair A. Therefore, the function generator was "loaded" to a lesser extent, which ultimately led to a higher voltage reading across the strips. For the specimen and standard of pair B, the RMS voltage was measured to be 4.3 V. This produced 14 mA of current through each strip and thus a power dissipation and heat flux of 60 mW and 0.6 W/cm^2, respectively. The larger signal can be attributed to an increase in dissipated power resulting from a larger current flow through the strip.

A plot of corrected phase data for specimen pair B is shown in Fig. 5.4. Again, the experimental data is represented by open symbols and the curves passing through the data points resulted from the curve fitting routine. Figure 5.4 shows that a thinner strip did produce a closer fit between the experimental phase data and the analytical model at each of the frequencies studied. However, the correlation at the 500 Hz data points was still insufficient.

Each curve of Fig. 5.4 represents a single temperature with thermal properties as determined by the fitting routine. Analogous to the results for specimen pair A, a single curve is associated with one thermal diffusivity and two effusivities, each corresponding to the silicon thermal conductivity that was used in the fitting routine. From these two properties, the thermal conductivity and specific heat of the thin film were calculated. The resulting thin film properties are plotted in Figs. 5.5 and 5.6, respectively, and are also given in Table 5.1. The vertical hatch marks between the two curves of a figure represent an uncertainty band due to uncertainty in the thermal conductivity of the silicon substrate. The nominal value of this property was altered simply to show the relative effect that a single property would have on the final results.

The solid black lines of Figs. 5.5 and 5.6 represent a recommended set of values for thermal conductivity[22] and specific heat[4] of fused silica in bulk form. The properties that were calculated by using the experimental data of specimen pair B were consistent with past work on fused silica.[3,21] The thermal conductivity of the film fell below the bulk values and the specific heat closely resembled that of bulk. Although a reduction in nichrome thickness brought the experimental data closer to the values predicted by the analytical model, a better correlation was still sought.

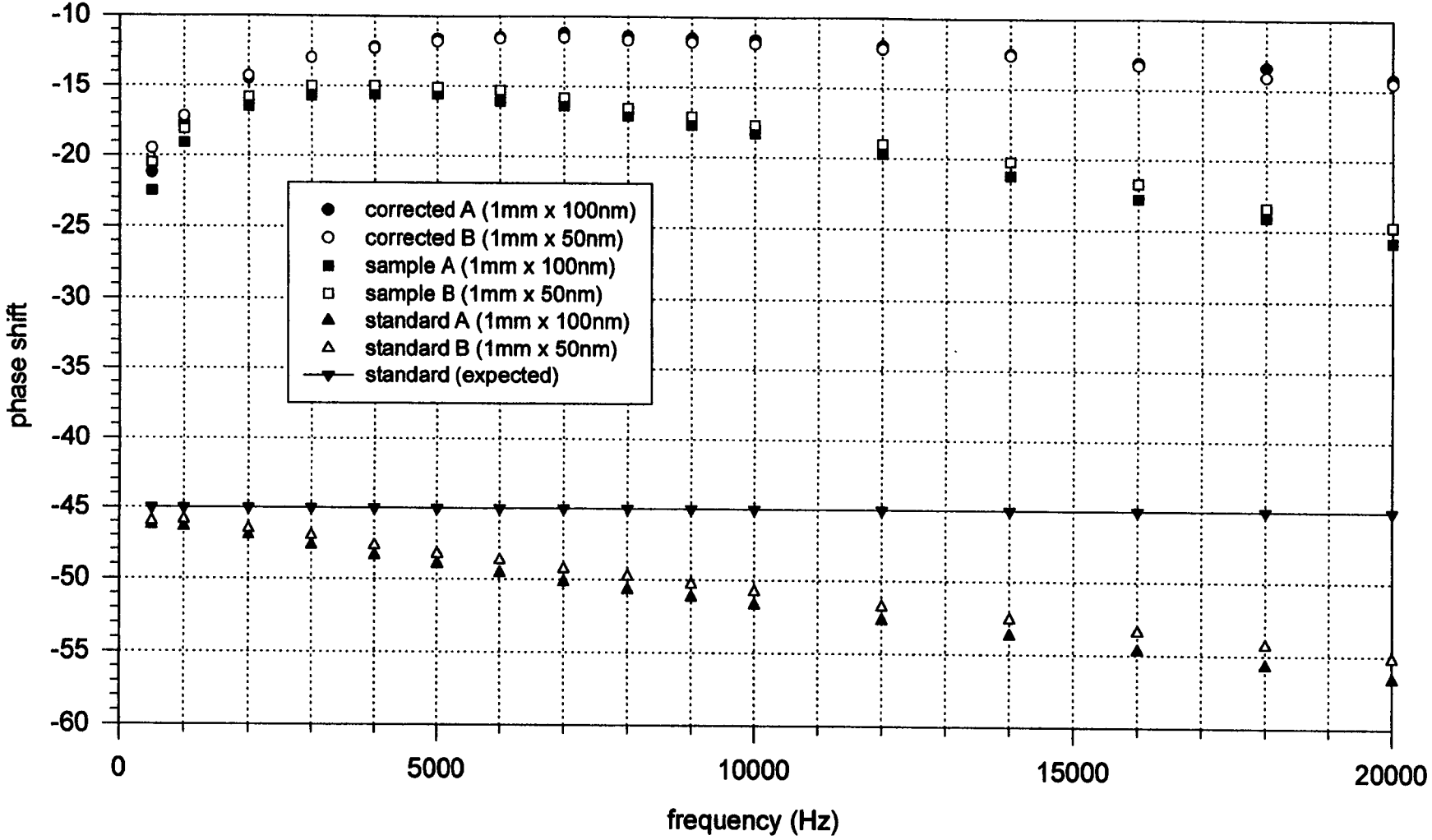

Figure 5.2 Phase Comparison: 50 nm and 100 nm Heating Strip

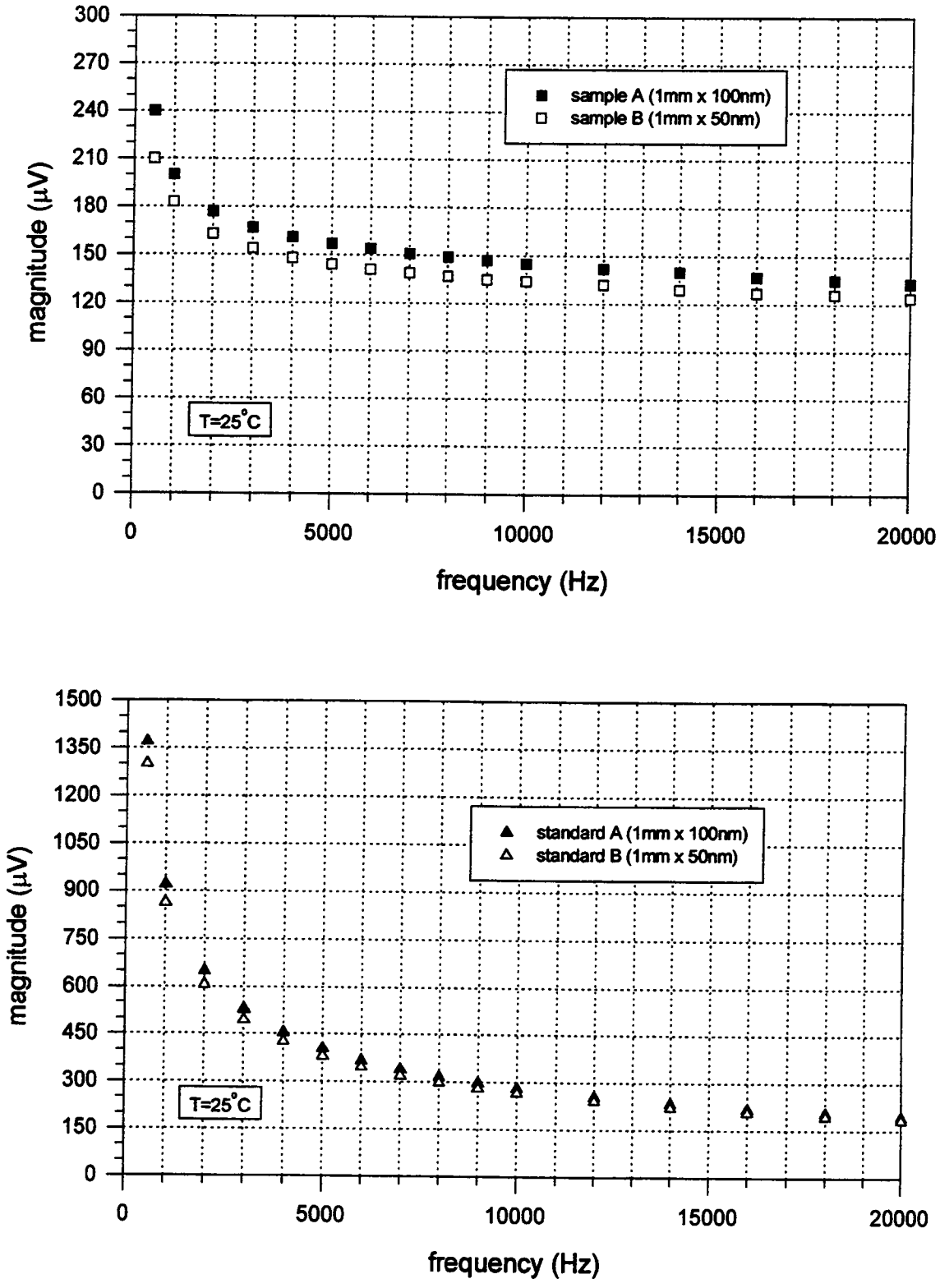

Figure 5.3 Magnitude Comparison: 50 nm and 100 nm Heating Strip

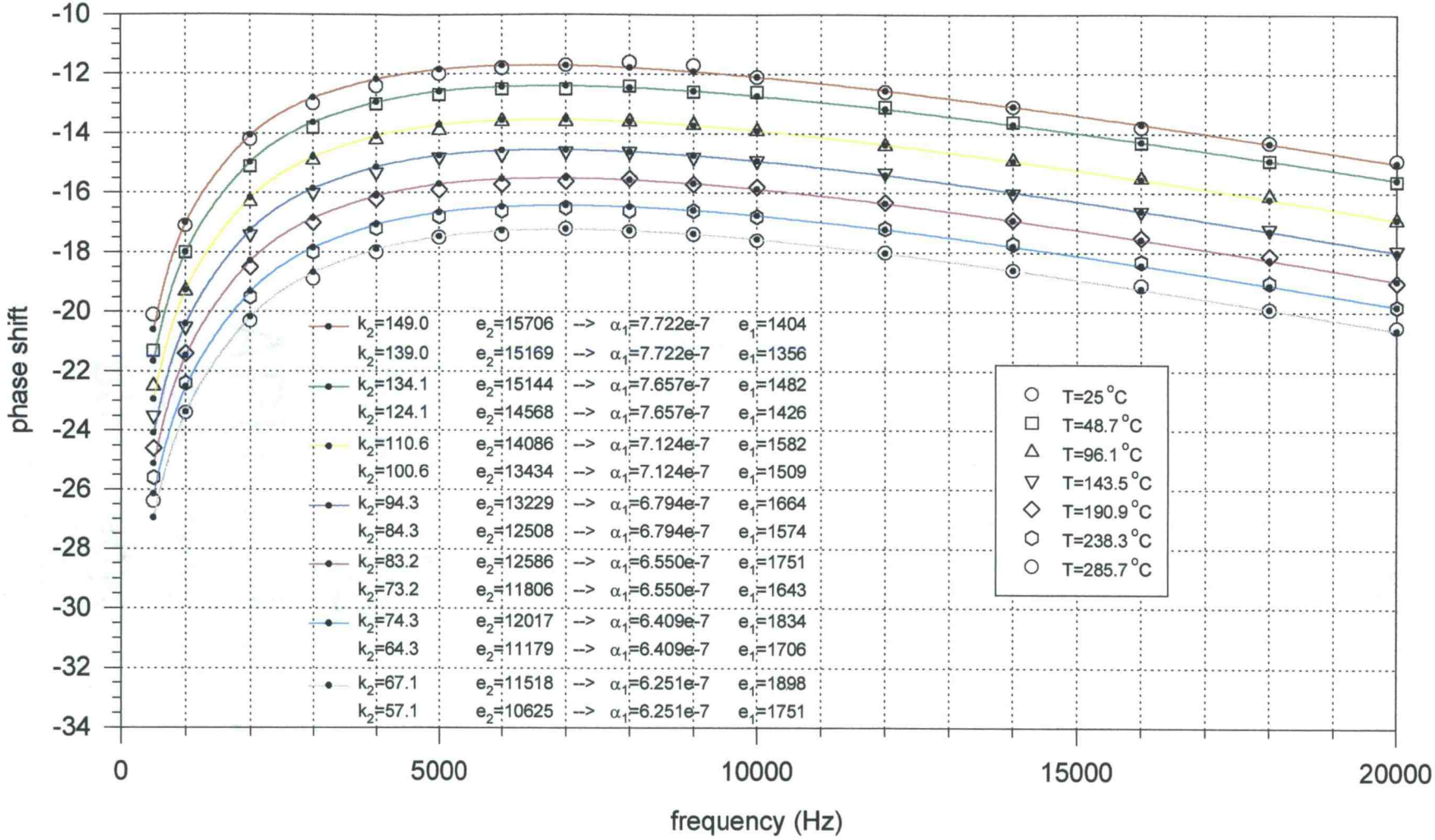

Figure 5.4 Curve Fit Results: Specimen Pair B

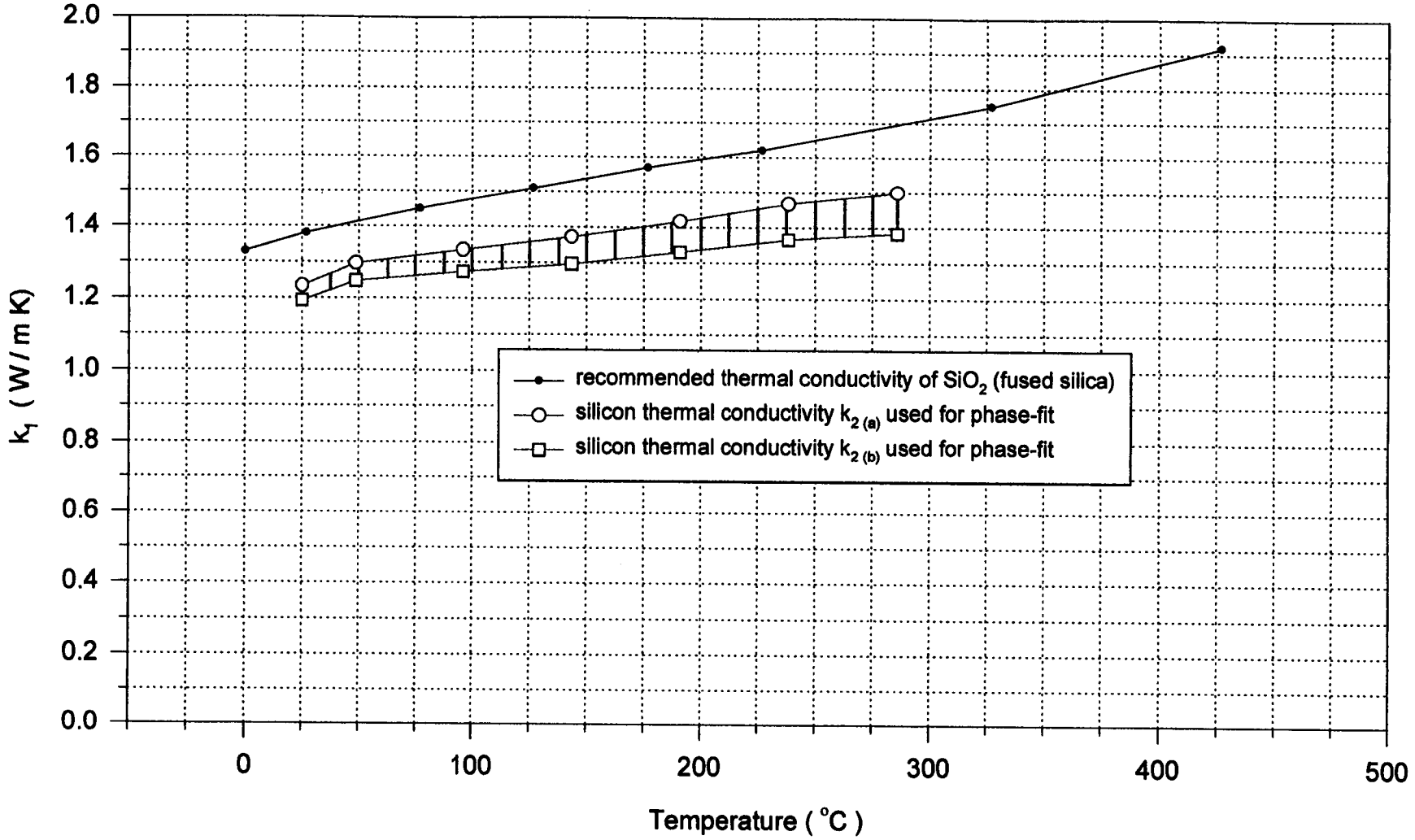

Figure 5.5 Thermal Conductivity: Specimen Pair B

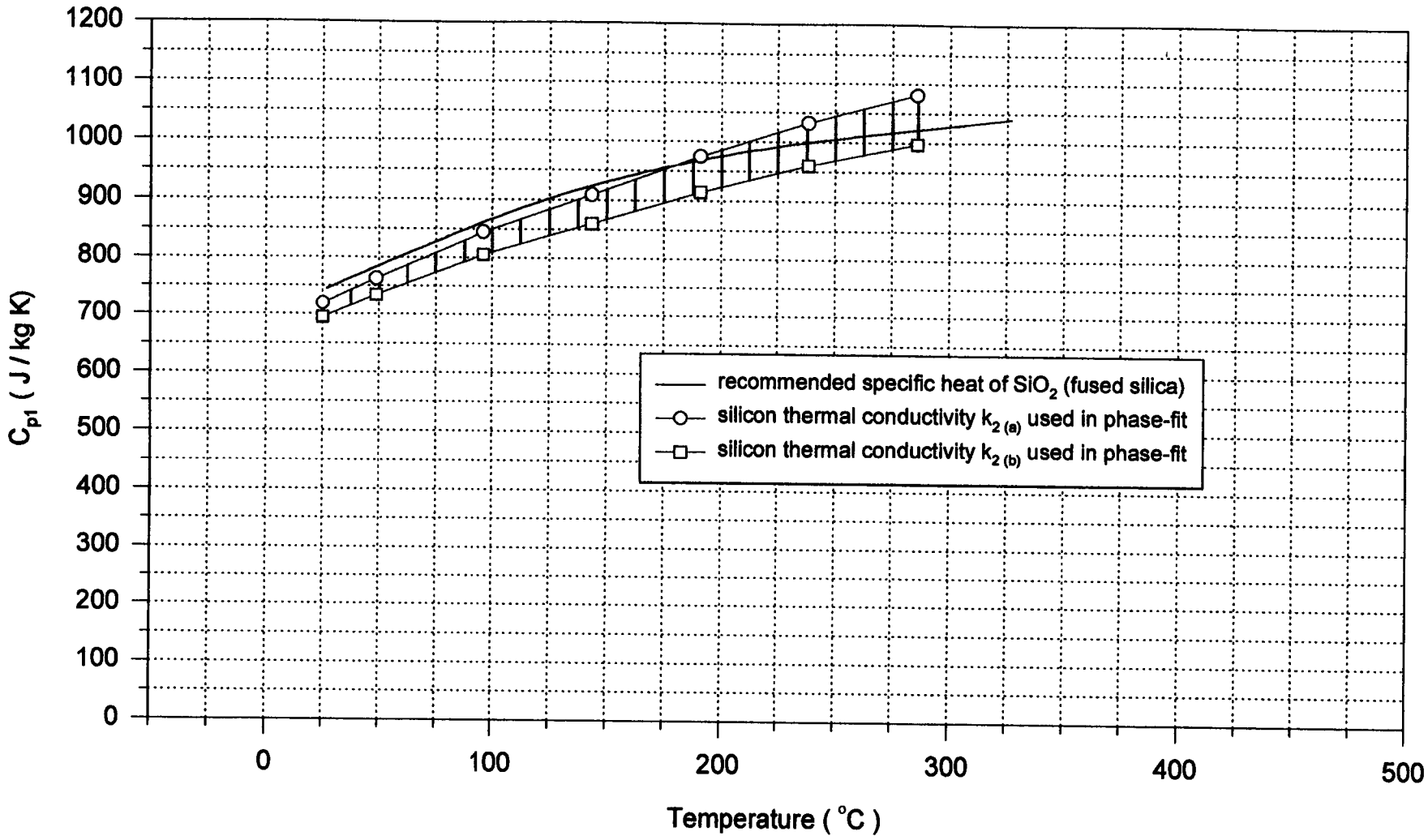

Figure 5.6 Specific Heat: Specimen Pair B

5.3. Specimen Pair C : 2 mm x 50 nm

In order to bring the corrected low frequency data points closer to values predicted by the analytical model, a different nichrome configuration was tried. Specimen pair C was fabricated with the idea that a wider heating strip would produce better results at low frequencies by reducing one dimensional 'edge effects' possibly present at the nichrome boundaries. The results presented in previous sections of this chapter were for specimen pairs with a 1 mm wide strip. Note that the detector element was of the same width. Even if edge effects were not a factor, the optical system would have to be in perfect alignment to produce an optimal signal at the detector output. Therefore, if the system had not been perfectly aligned, non-uniform heating at the nichrome edges would only degrade the signal further.

With specimen pair C in the sample holder, the emitting nichrome surface was twice as wide as the detector element. With proper focusing, the detector only imaged the middle of the strip, thus minimizing the edge effects. The phase data obtained with this specimen pair were in excellent agreement with the analytical model at all frequencies and each temperature studied. The corrected data is shown in Fig. 5.7. Again, a single diffusivity value and two effusivity values resulted from the fitting routine for each temperature, depending on the chosen silicon thermal conductivity. The film's thermal conductivity and specific heat were calculated using the results of each fit. These properties are plotted in Figs. 5.8 and 5.9, respectively, and are also given in Table 5.1. The hatched area represents an uncertainty band due exclusively to the thermal conductivity value chosen for the silicon substrate. The single solid black line in each figure represents a recommended set of values for thermal conductivity[22] and specific heat[4] of fused silica in bulk form. Similar to specimen pair B, the results for thermal conductivity and specific heat determined with specimen pair C were consistent with past work on SiO_2 films.[3,21] However, unlike the phase data of the previous specimen pairs, the data for this pair was well represented by the analytical model at all frequencies, including 500 Hz. Therefore, the thermal properties that resulted from its use provide the best representation of the SiO_2 film studied.

Although the correlation between the 500 Hz data points of specimen pair C and the analytical model had significantly improved, seven out of ten of the data points (corresponding to the various temperatures) were still slightly higher than the analytical model's predicted values. This result is likely due to the resolution of the digital readout on the lock-in's display, in that phase shift could only be recorded to within $\pm 0.1°$. Resolution is discussed within the uncertainty analysis section to follow. A different explanation is provided below.

If not due to experimental error, another possible reason for the slight mismatch between the data points at 500 Hz and the analytical model is that the assumption of a semi-infinite substrate was not entirely valid. A thermal diffusion length was discussed in chapter three of this paper and it was shown that frequencies in excess of 500 Hz were adequate to ensure that the semi-infinite solid assumption was valid when recording data for the fused silica standard. However, assuming that the silicon substrate was a semi-infinite medium may not be justifiable.

Because the thickness of the silicon substrate is much larger than the film thickness, a diffusion length was calculated by neglecting the film altogether. The diffusivity of silicon is approximately 8.92×10^{-5} m^2/s at 25°C. By using this value for diffusivity along with a heating frequency of $\omega = 2\pi 500$, the thermal diffusion length for the silicon substrate becomes $\mu = 2.383 \times 10^{-4}$ m. When multiplied by a value of 2π, the distance into the solid where the thermal wave has been effectively dampened becomes 1.497×10^{-3} m. Recall that the thickness of the silicon substrate was only 0.675×10^{-3} m, which is less than half of the penetration depth calculated above. However, at a distance of only π times the thermal diffusion length, the amplitude of the thermal wave has been reduced by over 90%. Although not fully dampened, the thermal wave would be substantially weaker at the back surface of the substrate when the nichrome strip was excited by a frequency of 500 Hz. It is therefore considered unlikely that the front surface phase data would be significantly altered by the finite substrate thickness, and the use of a semi-infinite medium in the analytical model was valid. The extremely close match between the data points and analytical model over the entire frequency range provide validation to such a conclusion.

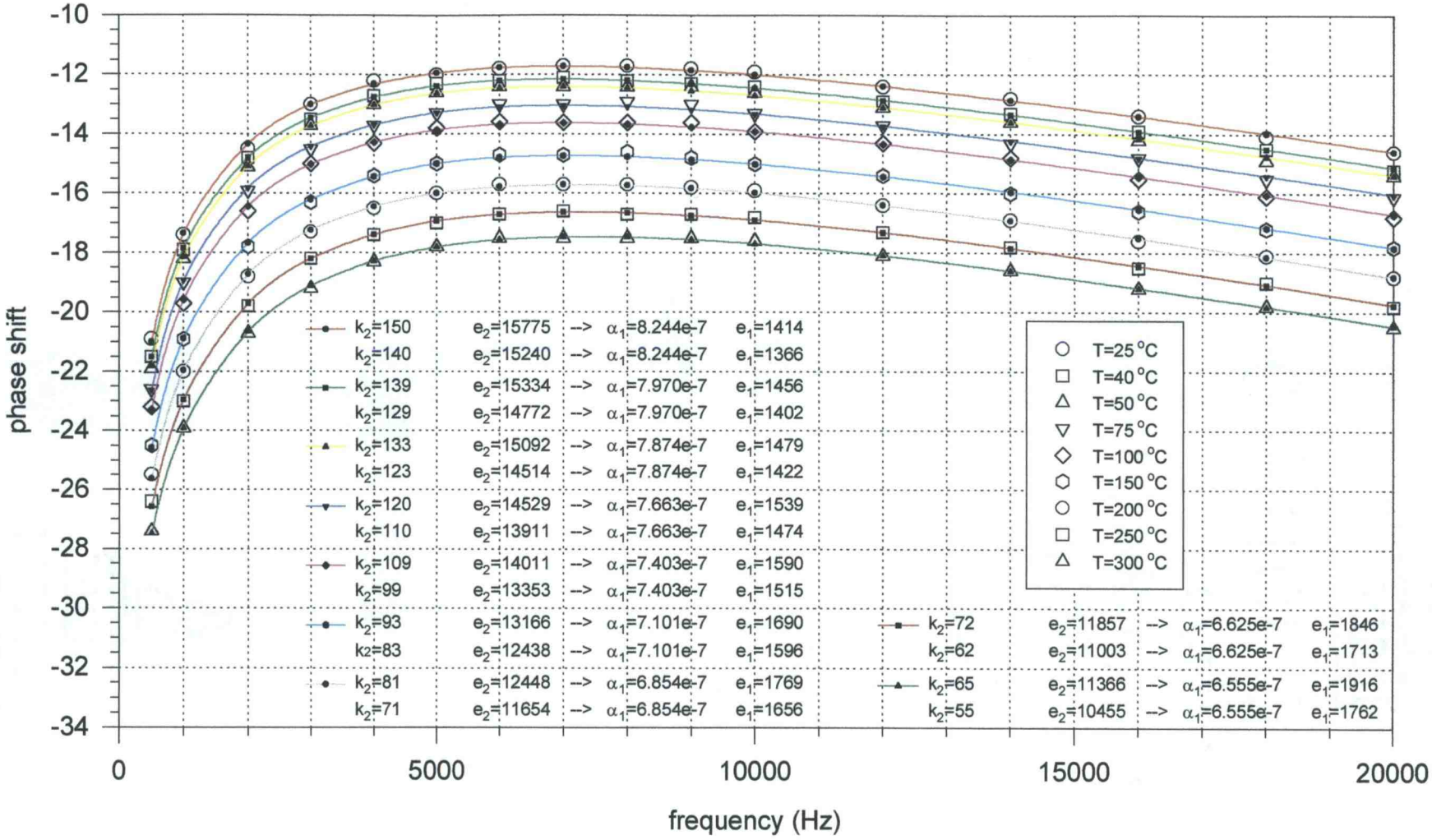

Figure 5.7 Curve Fit Results: Specimen Pair C

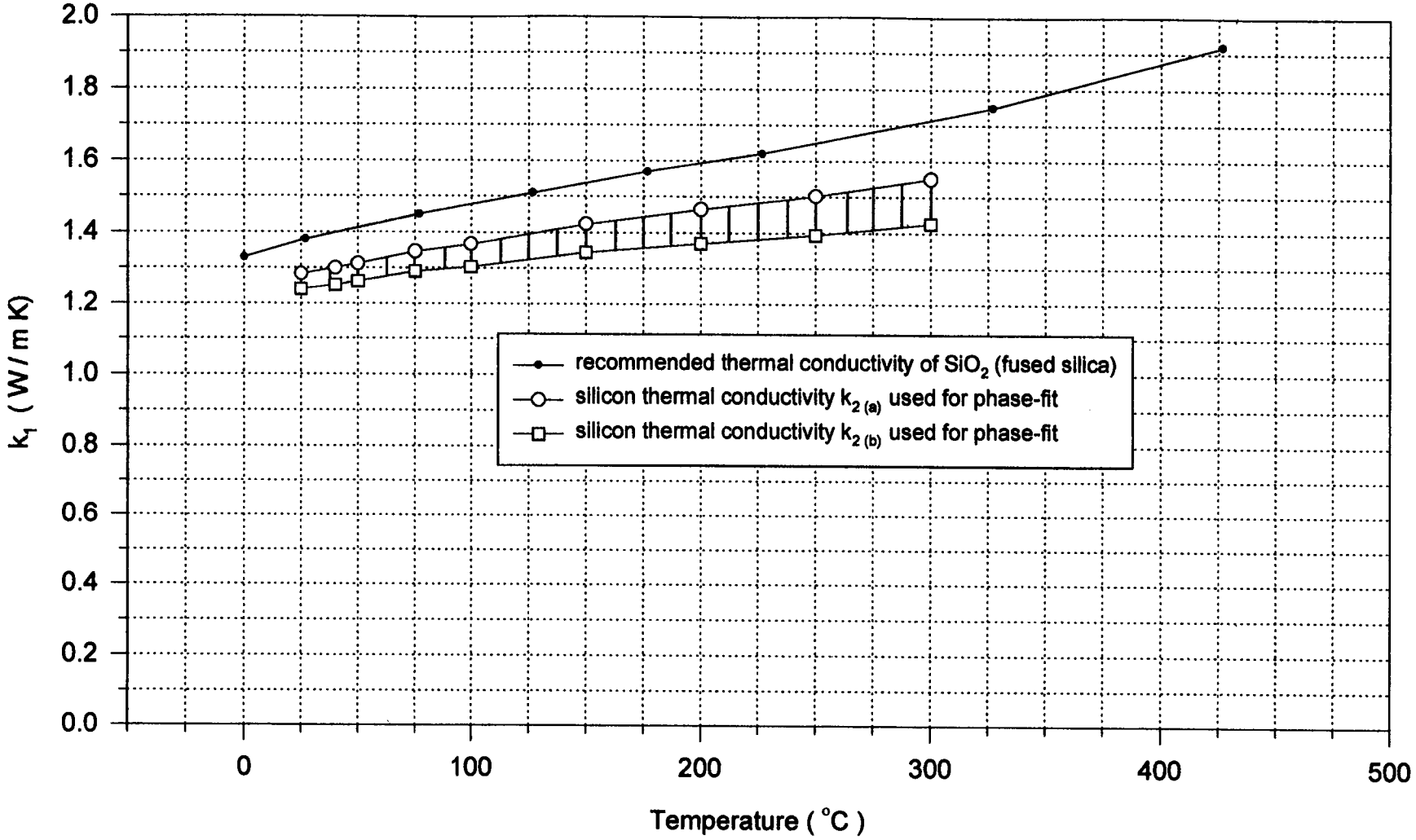

Figure 5.8 Thermal Conductivity: Specimen Pair C

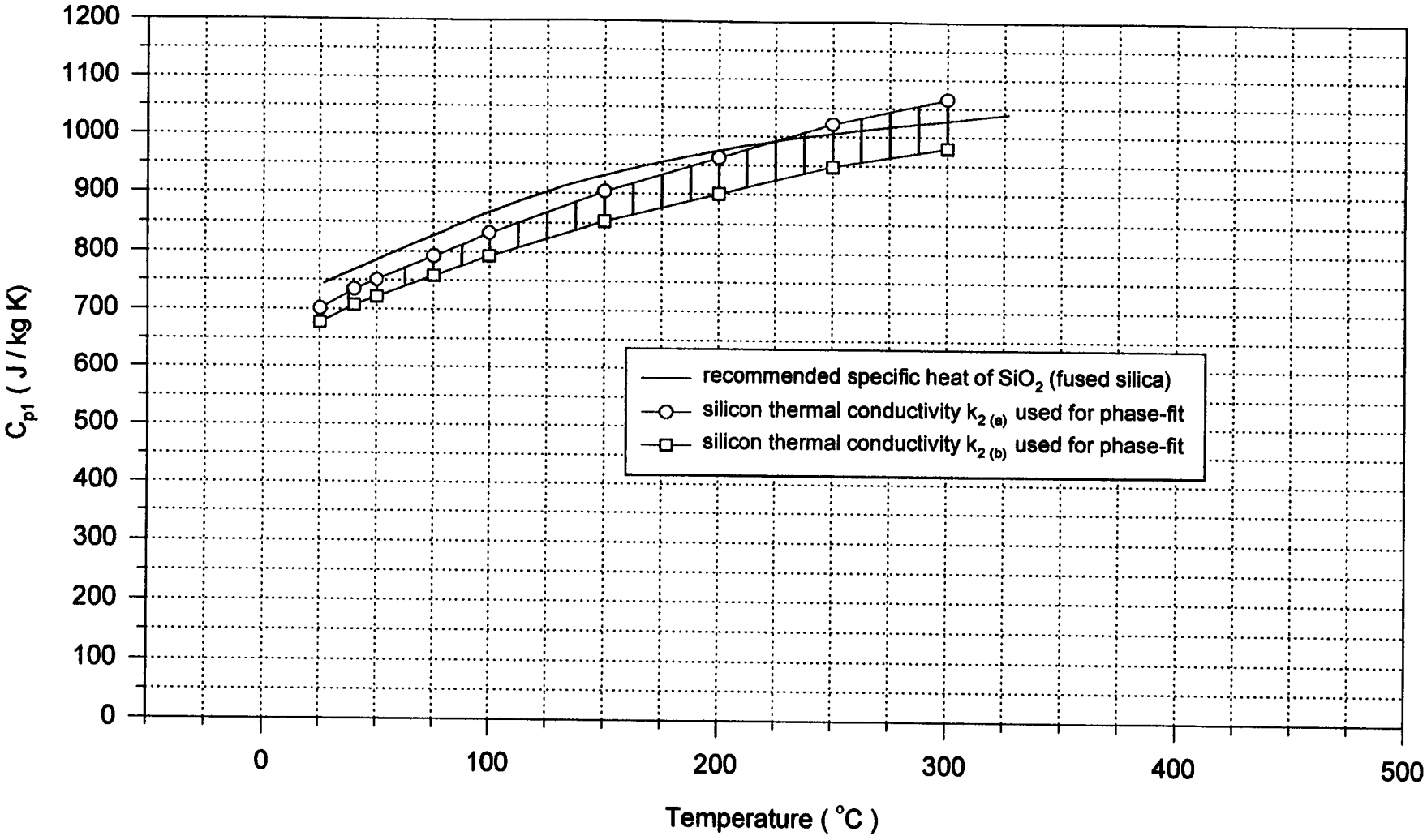

Figure 5.9 Specific Heat: Specimen Pair C

5.4. Specimen Pair C* : 2 mm x 50 nm + Nickel

Through studies of specimen pairs B and C at temperatures above 200°C, the formation of an oxide layer on the entire nichrome surface was encountered. The copper shims used between each contact rod and contact pad also became heavily oxidized at these temperatures. Although the oxide formation never caused problems during a frequency sweep with the system at an elevated temperature, problems did arise when the sample was cooled to room temperature and then taken back to a temperature at which data were desired. In some cases, the oxide formation was large enough to prevent adequate contact between the contact rod and nichrome contact pad. This usually resulted in a severely degraded heating signal or sometimes no signal at all. In either case, the specimen pair was no longer useful and had to be discarded.

Nickel was incorporated into specimen pair C* in order to decrease the formation of oxide at the points of electrical contact. This specimen pair had heating strips that were identical to those of specimen pair C. However, a 50 nm layer of nickel had been deposited on top of each nichrome contact pad. The 2 mm wide portion of the nichrome heating strip was left exposed to the atmosphere. Nickel shims were also used between the contact rods and contact pads in place of copper.

With the new specimen pair in the sample holder, the pair was taken up to temperatures of 100°C, 200°C, and 300°C, respectively. At each of these temperatures, the phase data produced at the lock-in was compared to the phase data that had been recorded for specimen pair C. A close match was found at all frequencies, which showed that the system was producing reliable data. The system was then allowed to sit at 300°C for approximately one hour, after which it was cooled to room temperature. When the pair was taken out of the sample holder and studied, it was apparent that oxide formation had been reduced on the modified nickel contact pads. This was a pleasing result, but much larger reduction in oxide formation was found on the shims. In past experiments, severe discoloration of the copper shims was encountered after the apparatus had been taken to elevated temperatures. Surprisingly, no visible discoloration was apparent when the nickel shims were examined.

An oxide layer still formed on each nichrome surface that was exposed to the atmosphere. A thin layer of oxide on the emitting surface is not expected to produce a significant effect on phase information. However, if accurate magnitude data were required for the determination of thermal properties, the formation of an oxide layer on the nichrome heating strip would be of concern.

Upon cool down, it was possible to maintain suitable electrical contact between the contact pads and contact rods of the standard and sample of specimen pair C^*. When the resistance values of this pair were measured, it was found that oxidation did not produce a significant barrier between the contact rod and nickel pad. A resistance reading for each strip was easily attainable, and values measured prior to heating were comparable to those found upon cool down (within a few ohms). This was not the case upon cool down of the specimen pair with bare nichrome used as contact pads. It was not possible to maintain adequate electrical contact on the nichrome pads of specimen pair C after the pair had been taken to elevated temperatures. Thus, the resistance of the nichrome strip could not be obtained for the sample of this pair, nor the standard. No quantitative results for thin film thermal properties are presented for specimen pair C^*, but the use of nickel has shown one promising solution for minimizing the formation of oxide on an important system component.

5.5. Uncertainty Analysis

All of the values obtained experimentally for the thermal conductivity and the specific heat of each thin film sample are summarized in Table 5.1. The table displays results grouped into three regions (A, B, C), with each representing one of the specimen pairs presented with qualitative data. For each pair, the values used in the fitting routine for the thermal conductivity and the specific heat of the silicon substrate are given as a function of temperature. The larger substrate conductivity was used as the 'nominal' value. The thin film properties that were calculated with experimental data from the measurement system are found next to the appropriate silicon properties.

Table 5.1 Thin Film Thermal Conductivity and Specific Heat

		Substrate (Si)		Thin Film (SiO_2)	
	T (°C)	k_2 (W / m K)	C_{p2} (J / kg K)	k_1 (W / m K)	C_{p1} (J / kg K)
A	25	149.0	710.5	1.325	651.3
		139.0		1.279	628.7
B	25	149.0	710.5	1.234	719.7
		139.0		1.192	695.1
	48.7	134.1	734.0	1.297	762.9
		124.1		1.248	734.1
	96.1	110.6	770.0	1.335	844.3
		100.6		1.274	805.3
	143.5	94.3	796.5	1.372	909.4
		84.3		1.297	860.2
	190.9	83.2	817.2	1.417	974.6
		73.2		1.330	914.5
	238.3	74.3	834.2	1.468	1031.9
		64.3		1.366	959.9
	285.7	67.1	848.6	1.501	1081.4
		57.1		1.384	997.6
C	25	150	712.0	1.284	701.5
		140		1.240	677.7
	40	139	726.0	1.300	734.6
		129		1.252	707.4
	50	133	735.0	1.312	750.8
		123		1.262	721.9
	75	120	755.0	1.347	791.9
		110		1.290	758.5
	100	109	773.0	1.368	832.4
		99		1.304	793.2
	150	93	800.0	1.424	903.4
		83		1.345	853.1
	200	81	821.0	1.465	962.5
		71		1.371	901.0
	250	72	838.0	1.503	1021.6
		62		1.394	948.0
	300	65	853.0	1.551	1066.0
		55		1.427	980.3

It has been recognized that uncertainty exists within several elements of this measurement technique, and that the uncertainty associated with a single system element will propagate toward uncertainty in the final results for thin film thermal properties. To place an estimate on how far the thermal conductivity and specific heat might differ from the 'nominal' values as a result of uncertainty, two situations were investigated. First, uncertainty in the experimental phase data was examined. Then, uncertainty associated with each variable used in the fitting routine was studied. The motivation here was to place an estimate on an upper and lower bound for the thin film properties that have been calculated with this measurement technique. The film properties that were found by applying the nominal values of silicon in the fitting routine have been used as a baseline for comparison.

As with data obtained by any measurement system, uncertainty was inherent in the phase data produced using this procedure. The phase shift at the lock-in output was not expected to be in exact agreement with the physical phenomena occurring at the surface of the sample. However, it was hoped that this difference could be kept to a minimum by using the standard. Therefore, the uncertainty in phase data was expected to result solely from the resolution in a reading taken at the lock-in's digital display. Any experimental error remaining was constructively 'canceled' upon correction of the sample data with the data of the standard.

During experimentation it was found that random fluctuations at the lock-in display enabled a reading of phase shift that could be resolved within $\pm 0.1°$. A simple test was performed using this knowledge. The data obtained from specimen pair C (300°C) was used to show the possible effect that an error in phase shift might have on the final film properties calculated. To do this, each of the corrected values for phase shift was offset by twice the observed resolution, or $+0.2°$. The shifted data was then fit to the analytical model using the nominal properties of silicon in the routine. From these results, the thermal conductivity and specific heat of the film were calculated. The properties that were determined with the offset phase data differed from properties determined with the actual data by less than 2%. It was felt that an uncertainty of such a small magnitude was insignificant in the overall measurement scheme.

Next, the data of specimen pair C was studied in order to place an uncertainty estimate on the resulting film properties due to uncertainty in the variables used in the fitting routine. The variables explored were film thickness (L), thermal conductivity of silicon (k_2), specific heat of silicon (C_{p2}), density of silicon (ρ_2), and the film density (ρ_1). As pointed out in a previous chapter, a literature survey on the thermal conductivity of silicon as a function of temperature produced a range of values with up to 10% variation.[18,19] Although it had not been as well characterized, similar property variation was found in the specific heat of silicon as a function of temperature.[20] Possible contributors to such property variation are doping level and measurement technique. With this in mind, the thermal properties of silicon were allowed to vary by 10% from their nominal values in the analysis presented in the following paragraphs. On the other hand, density was considered as a well characterized material property. The density of both the fused silica film and the silicon substrate were not expected to stray from their respective bulk values by more than a few percent. Therefore, a conservative bound of 5% was placed on the possible variation in density for both the silicon substrate and the thin film of fused silica. Finally, considering inaccuracy associated with the measurement of film thickness, this experimental quantity was assigned an uncertainty of 5% with respect to its nominal value of 1.72 μm.

A change in each of the five 'variables' above was examined at the temperatures of 25°C, 100°C, 200°C, and 300°C to show the effect that each had on the final thin film thermal properties. Thus, a total of twenty separate fits were required. Five fits were carried out at each temperature, one for every property. In any given fit, four of the variables were held to their nominal values and the fifth variable was altered by the percentage stated above. The thermal properties of the thin film were calculated with the fit results and each property was then compared to that calculated when nominal values for all five variables were used.

A simple RSS (Root-Sum-Square) technique was used on the 'error' associated with each variable at the four temperatures studied. For instance, by using the nominal value of each variable at 25°C, a nominal value of 1.284 W/m K was produced for the thin film thermal conductivity. When the silicon substrate's thermal conductivity was

varied by 10% while holding all other properties to their nominal values, the fit produced a new value of 1.218 W/m K for the film conductivity. The new value was 0.065 W/m K less than the nominal. This difference was considered as the 'error'. Similarly, by varying the substrate density, substrate specific heat, film thickness, and film density, the film thermal conductivity produced by each fit was 1.251 W/m K, 1.218 W/m K, 1.217 W/m K, and 1.284 W/m K, respectively. The magnitude of the offset of each from the nominal conductivity was calculated to be 0.033 W/m K, 0.065 W/m K, 0.067 W/m K, and finally 0.000 W/m K. Note that film density does not effect the result for conductivity. Density effectively cancels when using the curve fitting results together with Eqs. (3.88) and (3.89). The RSS technique was then used,

$$\text{RSS} = \sqrt{0.065^2 + 0.033^2 + 0.065^2 + 0.067^2 + 0.000^2} = 0.118\ \text{W/m K} \qquad (5.1)$$

From the above calculation, the final value of thin film thermal conductivity at a temperature of 25°C becomes 1.284 ± 0.118 W/m K. In other words, the true value of the thermal conductivity at 25°C is not expected to deviate more than 9.2% from the nominal value. This method was repeated for the remaining properties of thin film thermal conductivity and specific heat. The properties used in the analysis, along with the resulting film properties and corresponding 'error' are presented in Table 5.2. Through this analysis, it was determined that the error associated with each variable propagates toward an uncertainty no larger than 10% from the nominal film properties.

It has been shown that small errors in experimental phase data do not have a significant effect on the thin film thermal characterization. On the other hand, a small change in each variable used within the curve fitting routine does have a significant effect on the outcome of thermal property calculations. After taking into account uncertainty in the entire technique, it is therefore estimated that the true thin film thermal properties can be found within a band no larger than $\pm 10\%$ from the nominal values previously calculated. The nominal properties for the fused silica thermal conductivity and specific heat are shown in Figs. 5.9 and 5.10, respectively, along with error bars produced from the uncertainty analysis presented in this section.

Table 5.2 Uncertainty Analysis: Phase Data from Specimen Pair C

		k_2 ± 10%		ρ_2 ± 5%		C_{P2} ± 10%		L ± 5%		ρ_1 ± 5%						RSS			RSS
		nominal	10%	nominal	5%	nominal	10%	nominal	5%	nominal	5%	e_1	α_1	C_{P1}	'error'	↓	k_1	'error'	↓
25°C		**150**	135	**2330**	2213.5	**712**	640.8	**1.72E-06**	1.63E-06	**2220**	2109	1414	8.244E-07	701.5	0.0		1.284	0.000	
	1	150	135	2330	2213.5	712	640.8	1.72E-06	1.63E-06	2220	2109	1342	8.244E-07	665.8	35.7		1.218	0.065	
	2	150	135	2330	2213.5	712	640.8	1.72E-06	1.63E-06	2220	2109	1378	8.244E-07	683.6	17.9		1.251	0.033	
	3	150	135	2330	2213.5	712	640.8	1.72E-06	1.63E-06	2220	2109	1342	8.244E-07	665.8	35.7	**75.7**	1.218	0.065	**0.118**
	4	150	135	2330	2213.5	712	640.8	1.72E-06	1.63E-06	2220	2109	1414	7.404E-07	740.2	-38.7		1.217	0.067	
	5	150	135	2330	2213.5	712	640.8	1.72E-06	1.63E-06	2220	2109	1414	8.244E-07	738.4	-36.9		1.284	0.000	
		k_2 ± 10%		ρ_2 ± 5%		C_{P2} ± 10%		L ± 5%		ρ_1 ± 5%									
		nominal	10%	nominal	5%	nominal	10%	nominal	5%	nominal	5%	e_1	α_1	C_{P1}	'error'		k_1	'error'	
100°C		**109**	98.1	**2330**	2213.5	**773**	695.7	**1.72E-06**	1.63E-06	**2220**	2109	1590	7.403E-07	832.4	0.0		1.368	0.000	
	6	109	98.1	2330	2213.5	773	695.7	1.72E-06	1.63E-06	2220	2109	1508	7.403E-07	789.5	42.9		1.297	0.071	
	7	109	98.1	2330	2213.5	773	695.7	1.72E-06	1.63E-06	2220	2109	1550	7.403E-07	811.5	20.9		1.334	0.034	
	8	109	98.1	2330	2213.5	773	695.7	1.72E-06	1.63E-06	2220	2109	1508	7.403E-07	789.5	42.9	**90.3**	1.297	0.071	**0.128**
	9	109	98.1	2330	2213.5	773	695.7	1.72E-06	1.63E-06	2220	2109	1590	6.649E-07	878.3	-45.9		1.297	0.072	
	10	109	98.1	2330	2213.5	773	695.7	1.72E-06	1.63E-06	2220	2109	1590	7.403E-07	876.2	-43.8		1.368	0.000	
		k_2 ± 10%		ρ_2 ± 5%		C_{P2} ± 10%		L ± 5%		ρ_1 ± 5%									
		nominal	10%	nominal	5%	nominal	10%	nominal	5%	nominal	5%	e_1	α_1	C_{P1}	'error'		k_1	'error'	
200°C		**81**	72.9	**2330**	2213.5	**821**	738.9	**1.72E-06**	1.63E-06	**2220**	2109	1769	6.854E-07	962.5	0.0		1.465	0.000	
	11	81	72.9	2330	2213.5	821	738.9	1.72E-06	1.63E-06	2220	2109	1678	6.854E-07	913.0	49.5		1.389	0.075	
	12	81	72.9	2330	2213.5	821	738.9	1.72E-06	1.63E-06	2220	2109	1724	6.854E-07	938.0	24.5		1.427	0.037	
	13	81	72.9	2330	2213.5	821	738.9	1.72E-06	1.63E-06	2220	2109	1678	6.854E-07	913.0	49.5	**104.4**	1.389	0.075	**0.136**
	14	81	72.9	2330	2213.5	821	738.9	1.72E-06	1.63E-06	2220	2109	1769	6.155E-07	1015.7	-53.2		1.388	0.077	
	15	81	72.9	2330	2213.5	821	738.9	1.72E-06	1.63E-06	2220	2109	1769	6.854E-07	1013.2	-50.7		1.465	0.000	
		k_2 ± 10%		ρ_2 ± 5%		C_{P2} ± 10%		L ± 5%		ρ_1 ± 5%									
		nominal	10%	nominal	5%	nominal	10%	nominal	5%	nominal	5%	e_1	α_1	C_{P1}	'error'		k_1	'error'	
300°C		**65**	58.5	**2330**	2213.5	**853**	767.7	**1.72E-06**	1.63E-06	**2220**	2109	1916	6.555E-07	1066.0	0.0		1.551	0.000	
	16	65	58.5	2330	2213.5	853	767.7	1.72E-06	1.63E-06	2220	2109	1818	6.555E-07	1011.5	54.5		1.472	0.079	
	17	65	58.5	2330	2213.5	853	767.7	1.72E-06	1.63E-06	2220	2109	1867	6.555E-07	1038.7	27.3		1.512	0.040	
	18	65	58.5	2330	2213.5	853	767.7	1.72E-06	1.63E-06	2220	2109	1818	6.555E-07	1011.5	54.5	**115.3**	1.472	0.079	**0.144**
	19	65	58.5	2330	2213.5	853	767.7	1.72E-06	1.63E-06	2220	2109	1916	5.887E-07	1124.9	-58.9		1.470	0.081	
	20	65	58.5	2330	2213.5	853	767.7	1.72E-06	1.63E-06	2220	2109	1916	6.555E-07	1122.1	-56.1		1.551	0.000	

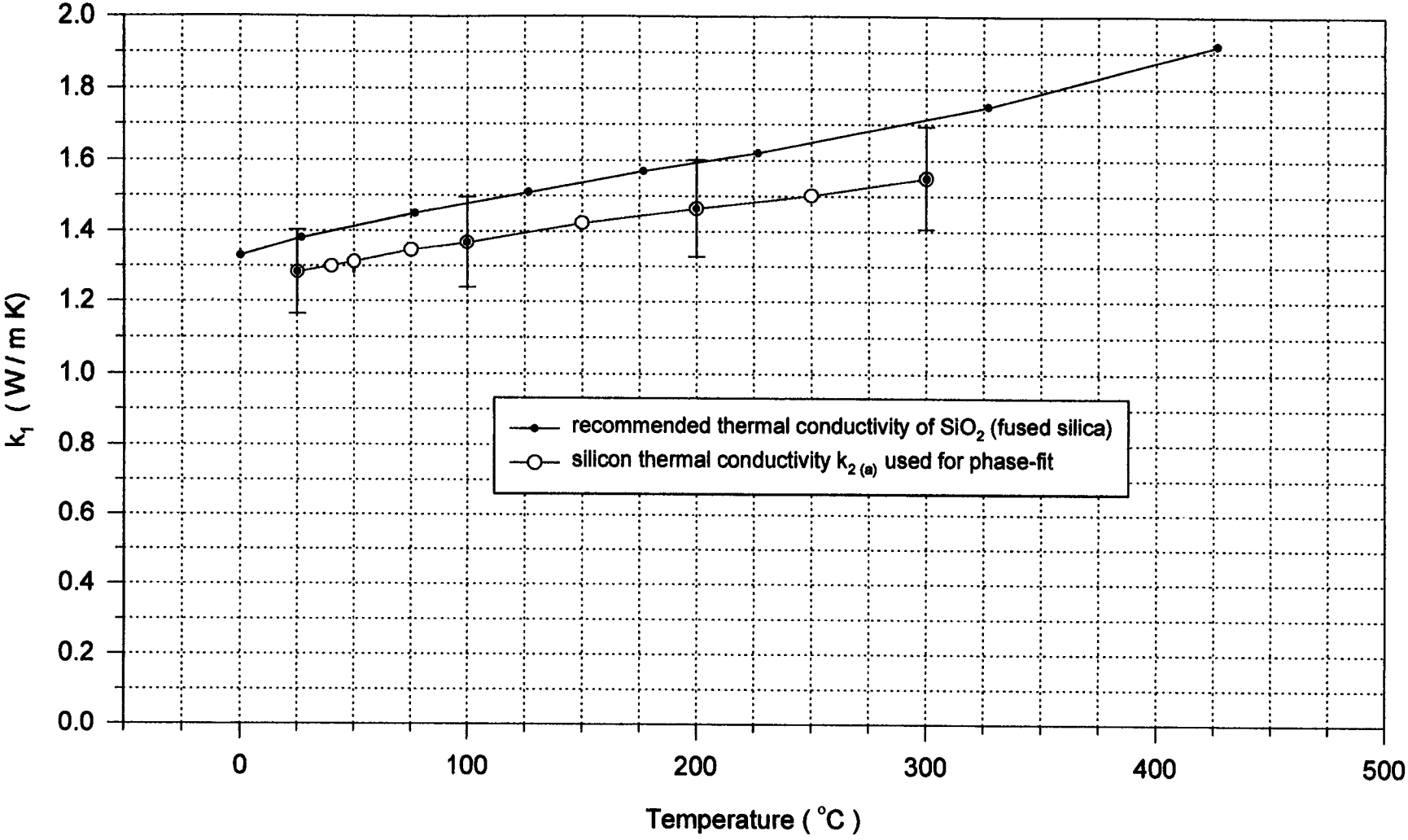

Figure 5.10 Uncertainty Estimate: Thermal Conductivity of Specimen Pair C

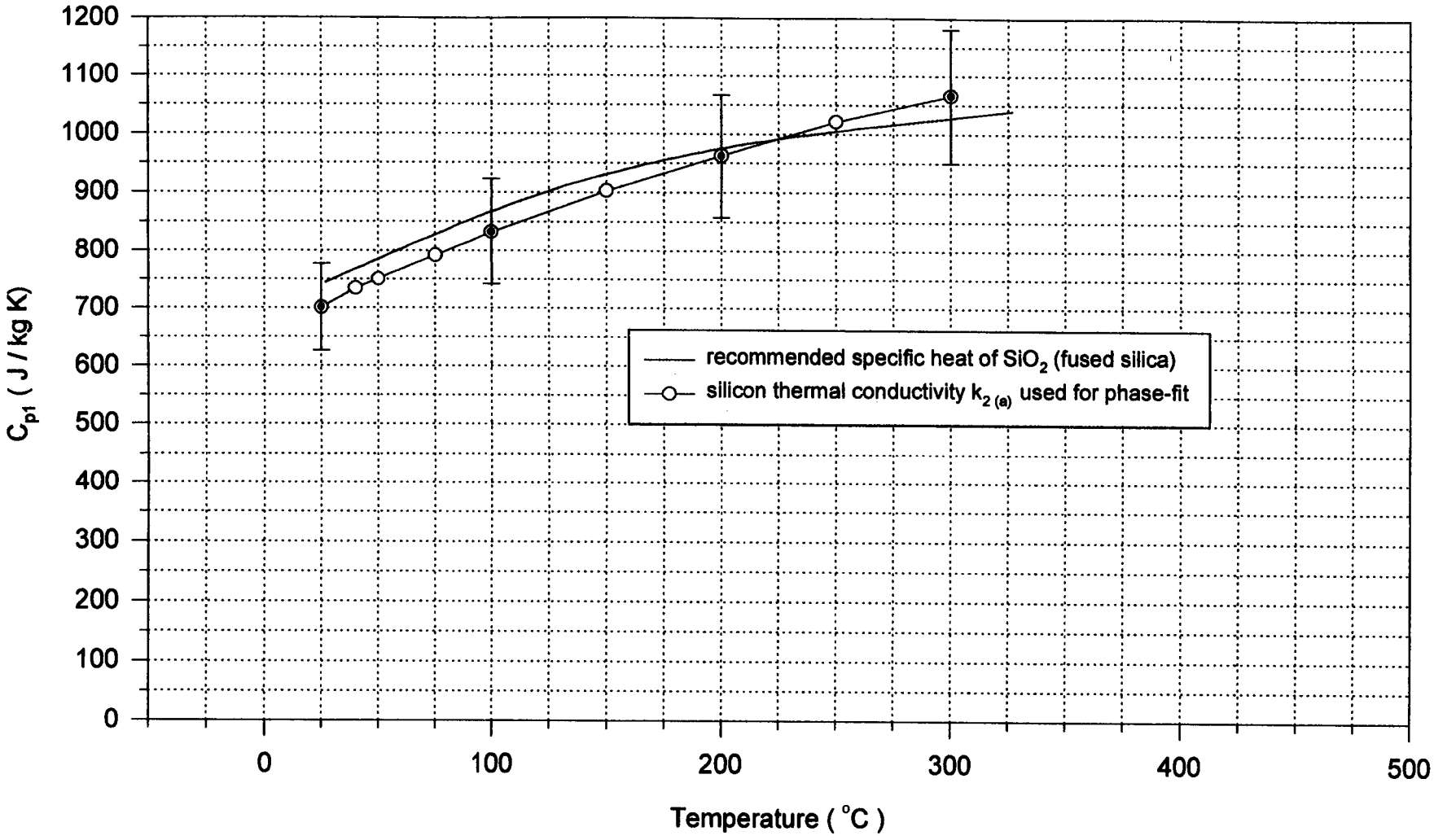

Figure 5.11 Uncertainty Estimate: Specific Heat of Specimen Pair C

5.6. Discussion

In past work on the determination of thin film properties, Decker *et al.*[21] found the thermal conductivity of fused silica films to be lower than bulk values by using a steady state method based on thermocouple measurements. They studied films that were fabricated using two deposition processes. Their measurements produced a thermal conductivity of 0.17 W/m K for a 1.05 μm thick e-gun evaporated film, which was less than the bulk value by a factor of 8. Also studied was a 0.50 μm thick reactively sputtered film of SiO_2 for which they measured a thermal conductivity of 0.28 W/m K. They concluded that film thermal conductivity depends strongly on deposition technique.

Lambropoulos *et al.*[3] have used a modified thermal comparator to determine the conductivity of various thin film materials with thicknesses between 0.50 μm - 4.40 μm. Their results showed a smaller effective conductivity for electron beam evaporated films of SiO_2 as compared to bulk values. Films that were fabricated from an ion beam sputtering process also produced conductivities that were lower than the bulk. The property values that were obtained with their method only differed from the bulk solid by a factor of approximately 3-5, in contrast to the factor of 8 found in the reference cited above. However, they have stated that uncertainty inherent within their method can affect the final film conductivity by up to a factor of two. Unlike the previous method, as well as the method presented here, they were able to provide an estimate for interfacial resistance along with film conductivity. They did not believe that thin film thermal conductivity was sensitive to the method of film preparation. Also noted was a strong dependence between film thickness and thermal conductivity for films of SiO_2 over the thickness range of 0.5 μm - 4 μm.

Silicon dioxide films that were fabricated with three different processes have been studied by Goodson *et al.*[23] The film thickness that they used ranged from 0.03 μm to 0.70 μm. Their work indicated that the fabrication process does have a strong influence on the conductivity of SiO_2 layers. Of great interest from the study were results found for a thermally grown film of SiO_2 with a thickness close to 0.5 μm. The

film's effective conductivity was determined to be approximately 1.27 W/m K. Although the film thickness was much smaller than the 1.72 μm thick film of the current work, the resulting thermal conductivity was extremely close to that presented for specimen pair C.

Thermally grown and chemical vapor deposited (CVD) silicon dioxide layers were also studied by Kading *et al.*[24] by using a non-contact technique. In their work, film thickness ranged from 20 nm to 200 nm. No significant dependence on thickness was observed, but it was found that the thermal conductivity of the CVD films was smaller than that of the thermally grown films. Their experiment involved a set of the thermally grown specimens with a 2 μm layer of gold sputtered on the top surface. For comparison purposes, another specimen had a 20 nm layer of chromium evaporated on its front surface prior to sputtering the 2 μm layer of gold. Two interfaces existed in a specimen, one at the silicon dioxide/silicon substrate boundary and the other at the silicon dioxide/metal boundary. They did not find a significant thermal boundary resistance at the silicon dioxide/silicon interface. However, they concluded that the thermal boundary resistance at the metal interface was strongly dependent on the metallization process, and was sometimes comparable to the internal resistance of the oxide layer itself.

The phase sensitive technique described in the present work has yielded values for the conductivity and specific heat of a thin silicon dioxide film (1.72 μm) at temperatures between 25°C - 300°C. The film was thermally grown and had a thin layer of nichrome on its top surface, thus two interfaces. It was determined that the thermal conductivity of the thin film was never more than 10% lower than the thermal conductivity of fused silica in bulk form over this temperature range. The results were in good agreement with previous work presented in the literature. Although the thermal conductivity values produced by this method were consistently lower than the bulk values, a larger variation has been reported for films fabricated by processes other than that used here. On the other hand, the values of specific heat that were found with the new method closely agree with the bulk values of fused silica, which was expected. No attempt was made at determining the extent of each interfacial

resistance. Thus, any such effects are embedded directly in the results presented. Each value of thermal conductivity that has been determined with this method should be viewed as an effective conductivity that includes possible contributions from a thermal boundary resistance at the heating strip/film interface and also the substrate/film interface.

6. CONCLUDING REMARKS

A phase sensitive measurement technique that permits the simultaneous determination of two independent thermal properties of a thin film has been presented. The technique is applicable to films of a dielectric nature, and has been applied effectively to 1.72 μm samples of fused silica between the temperatures of 25°C and 300°C. The technique involved heating the front surface of a sample with a periodic source while measuring the temperature response at the same location. The front surface temperature response was observed with an HgCdTe infrared detector, whose output signal was routed to a lock-in amplifier where phase information was produced. Phase shift was recorded for both a thin film sample and a fused silica standard. The standard was incorporated into the technique as a means for producing absolute phase data, thereby eliminating undesirable effects such as the finite response time of the electronic components within the system. The absolute phase data was then used in a fitting routine with the independent thermal properties of thermal diffusivity and effusivity used as fitting parameters. From the fit results, the thermal conductivity and specific heat of the fused silica thin film were determined. Finally, the resulting thermal properties were presented as a function of temperature along with corresponding values for uncertainty.

Because the sample was a film-on-substrate structure, various substrate properties were required in the fitting routine in order to obtain the thermal properties of the film. Also required in the routine were film thickness and film density. Therefore, it was recognized that the thin film thermal properties produced by the curve fit were only as good as the properties used in the fitting routine. A reasonable estimate for the uncertainty in each thin film thermal property that was determined by this method was approximated at 10% through an RSS uncertainty analysis. This percentage estimate for uncertainty was valid for both the thermal conductivity and the specific heat of the fused silica film over the entire temperature range studied. Through the use of this technique, it was found that the thin film thermal conductivity

was consistently lower than that of bulk fused silica. The same result has been widely presented in the literature. However, it seems that a smaller reduction in the thermal conductivity of thermally grown oxide layers can be expected as compared to equivalent oxide layers produced by many other fabrication techniques. It was also determined that the specific heat of the thin film was similar to that of the bulk solid. This result had been expected.

The literature has indicated that interfacial resistance may become increasingly important as film thickness decreases. As is, this technique neglects any thermal barrier that may be present at the thin film/substrate interface and also the thin film/nichrome interface. The effects of thermal resistance may be established in future studies. To do so, a thermal resistance could be incorporated into the analytical model, thus placing three 'unknowns' into the fitting routine. However, since the specific heat of a thin film is not expected to lie far from that of the bulk material, it could be specified directly in the routine, thus eliminating one of the unknowns. Another route that could be explored would be to run a number of curve fits for a single set of data while using a new value of thermal resistance in subsequent fits. If reasonable estimates are placed on thermal resistance, the resulting thermal properties could be used in a similar uncertainty analysis that was presented in this paper. By placing an estimate on uncertainty due to interfacial effects, it could be shown how the resulting film properties might be effected.

Another course that could be taken for future study comes in using a film of thickness other than that utilized here. It would be interesting to see results obtained for various fused silica films over a thickness range of 0.5 μm - 2 μm. However, reducing oxidation should be explored in more detail prior to any future thermal characterization efforts. The use of nickel provided promising results in this area, but should be further examined.

It is evident that there are many paths available for exploration with this experimental apparatus. Study of the present fused silica specimens has shown that the apparatus provides repeatable results and is straightforward to use. One drawback of the apparatus is the time required between turning the entire system on and

obtaining the desired steady heat sink temperature. However, the simplicity that comes with obtaining phase information at the lock-in makes up for this downfall. All in all, it is felt that the technique devised for thermal characterization of thin films has been a success, and its use should be considered for future studies.

BIBLIOGRAPHY

[1] Cengel, Y. A. *Heat Transfer: A Practical Approach*; McGraw-Hill: New York, 1998

[2] Lambropoulos, J. C.; Burns, S. J.; Jacobs, S. D.; Shaw-Klein, L. Effects of Anisotropy, Interfacial Thermal Resistance, Microstructure, and Film Thickness on the Thermal Conductivity of Dielectric Thin Films. ASME HTD-Vol. 227, **1992**, 37-49

[3] Lambropoulos, J. C.; Jolly, M. R.; Amsden, C. A.; Gilman, S. E.; Sinicrope, M. J.; Diakomihalis, D.; Jacobs, S. D. Thermal Conductivity of Dielectric Thin Films. *J. Appl. Phys.* **1989**, *66*, 4230-4242

[4] Incropera, F. P.; Dewitt, D. P. *Fundamentals of Heat and Mass Transfer*, 3rd ed.; Wiley & Sons: New York, 1990

[5] Taylor, R. Measurement of Thermal Properties. In *CRC Handbook of Thermoelectrics*, Rowe, D. M., Ed.; CRC Press: Boca, Raton, FL, 1995; Chapter 16.

[6] Cahill, D. G.; Fischer, H. E.; Klitsner, T.; Swartq, E. T.; Pohl, R. O. Thermal Conductivity of Thin Films: Measurement and Understanding. *J. Vac. Sci. Technol., A* **1989**, *7*, 1259-1266

[7] DeVecchio, D.; Russell, D.; Taborek, P. Measurement of Thermal Diffusivity of Small, High Conductivity Samples Using a Phase Sensitive Technique. *Rev. Sci. Instrum.* **1995**, *66*, 3601-3605

[8] Chen, G.; Tien, C. L. Thermal Diffusivity Measurement of GaAs/AlGaAs Thin-Film Structures, Presented at the ASME Winter Annual Meating, Nov. 28-Dec 3, New Orleans, Louisiana.

[9] Zhang, X.; Grigoropoulos, C. P. Thermal Conductivity and Diffusivity of Free-Standing Silicon Nitride Thin Films. *Rev. Sci. Instrum.* **1992**, *66*, 1115-1120

[10] Frank, R.; Drach, V.; Fricke, J. Determination of Thermal Conductivity and Specific Heat by a Combined 3w/Decay Technique. *Rev. Sci. Instrum.* **1993**, *64*, 760-765

BIBLIOGRAPHY (Continued)

[11] Bennett, C. A., Jr.; Patty, R. R. Thermal Wave Interferometry: A Potential Application of the Photoacoustic Effect. *Appl. Opt.* **1982**, *21*, 49-54

[12] Charpentier, P.; Lepoutre, F.; Bertrand, L. Photoacoustic Measurements of Thermal Diffusivity Description of the "Drum Effect". *J. Appl. Phys.* **1982**, *53*, 608-614

[13] Swimm, R. T. Photoacoustic Determination of Thin Film Thermal Properties. *Appl. Phys. Lett.* **1983**, *42*, 955-957

[14] Lachaine, A.; Poulet, P. Photoacoustic Measurement of Thermal Properties of a Thin Polyester Film. *Appl. Phys. Lett.* **1984**, *45*, 953-954

[15] Rosencwaig, A.; Gersho, A. Theory of the Photoacoustic Effect with Solids. *J. Appl. Phys.* **1976**, *47*, 64-69

[16] Meyers, G. E. *Analytical Methods in Conduction Heat Transfer*; McGraw-Hill: New York, 1971.

[17] Arpaci, V. S. *Conduction Heat Transfer*; Addison-Wesley: Reading, MA, 1966.

[18] Glassbrenner, C. J.; Slack, G. A. Thermal Conductivity of Silicon and Germanium from 3°K to the Melting Point*. *Phys. Rev.* **1964**, *134*, A1058-A1069

[19] Touloukian, Y. S.; Powell, R. W.; Ho, C. Y.; Klemens, P. G. Thermal Conductivity: Metallic Elements and Alloys. In *Thermophysical Properties of Matter-Vol. 1*, (IFI/Plenum Data Corporation, New York), 1970

[20] Touloukian, Y. S.; Buyco, E. H. Specific Heat: Metallic Elements and Alloys. In *Thermophysical Properties of Matter-Vol. 4*, (IFI/Plenum Data Corporation, New York), 1970

[21] Decker, D. L.; Koshigoe, L. G.; Ashley, E. J. Thermal Properties of Optical Thin Film Materials*. In *NBS Special Publication 727: Laser Induced Damage in Optical Materials.* 1984, (Government Printing Office, Washington, DC, 1986), 291-297

BIBLIOGRAPHY (Continued)

[22] Touloukian, Y. S.; Powell, R. W.; Ho, C. Y.; Klemens, P. G. Thermal Conductivity: Nonmetallic Solids. In *Thermophysical Properties of Matter-Vol. 2*, (IFI/Plenum Data Corporation, New York), 1970

[23] Goodson, K. E.; Flik, M. I.; Su, L. T.; Antoniadis, D. A. Annealing-Temperature Dependence of the Thermal Conductivity of LPCVD Silicon-Dioxide Layers. *IEEE Electron Device Lett.* **1993**, *14*, 490-492

[24] Kading, O. W.; Skurk, H.; Goodson, K. E. Thermal Conduction in metallized silicon-dioxide layers on silicon. *Appl. Phys. Lett.* **1994**, *65*, 1629-1631